Australian Government
Department of Defence
Defence Science and
Technology Organisation

# Development and Calibration of a Frangible Leg Instrumented for Compression and Bending

*M.J. Footner, D.M. Bergeron and R.J. Swinton*

**Weapons Systems Division**
**Defence Science and Technology Organisation**

DSTO-TR-1829

## ABSTRACT

In order to quantify the loads transferred to a human leg during a landmine explosion, the lower portion of the Frangible Surrogate Leg (FSL) was modified to incorporate a load sensor. This report describes these modifications and the work carried out to calibrate the response of the modified FSL (FSLM) to static and dynamic loads. Non-destructive drop tests were performed to characterise repeatability from test to test for a given specimen, as well as the variation of response between specimens. Upon completion of these calibrations, five FSLM specimens were subjected to the explosion of 50-gram PE4 charges buried in sand. The standoff between the specimens and the soil surface ranged from 50 mm to 200 mm. The results demontrated how variations of the explosive input affects the load transmitted to the specimens and the resulting level of damage.

*Published by*

*DSTO Defence Science and Technology Organisation*
*PO Box 1500*
*Edinburgh South Australia 5111 Australia*

*Telephone: (08) 8259 5555*
*Fax: (08) 8259 6567*


*AR-013-583*
*February 2006*

**APPROVED FOR PUBLIC RELEASE**

# Development and Calibration of a Frangible Leg Instrumented for Compression and Bending

## Executive Summary

This report summarises the work done to calibrate a modified Frangible Surrogate Leg (FSLM), which had been instrumented with strain gauges. Five FSLM specimens were subjected to non-destructive drop tests to develop a simple calibration equation for the compression force. The accuracy of the equation was verified by subjecting each FSLM to 200 mm drops several times. These drops generated a peak force around 4 kN at the reference load cell with a maximum load rate of approximately 500 kN/sec. The built-in load cell responded linearly to such input loads. However, the slope of the linear fits changed from one drop to the next, suggesting that a greater portion of the load was transmitted through the tibia after the first drop. It is surmised that this was due to a 'softening' of the glue joints that reduced the ability of the fibula to transfer its share of the vertical load. Comparing the calibration curves from one leg to the next revealed significant differences, up to 18%, in the slope for different legs. This result suggests that it is advantageous to calibrate each leg separately instead of using a generic calibration factor across multiple legs.

Once the non-destructive calibration process was completed, it was decided to subject the instrumented legs to varying explosive loads and to document the response of the FSLM. The method used to vary the explosive load was to always use the same setup of a 50-gram charge buried under 20 mm of sand, but to change the standoff between the FSLM and the charge. This approach proved to be an effective technique to control the strength of the explosive input into the FSLM. It produced peak loads that were up to 10 times greater than with the drop tests. The loading rate was also much larger, ranging from 50,000 to 270,000 kN/sec.

The physical damage to the footwear varied from superficial abrasions and tears at 200 mm to complete destruction of the heel region at 50 mm. The sole of the boot was breached at 125 mm. Additionally, the calcaneus and talus bones provided the most reliable response to the explosive inputs. The calcaneus was intact at 200 mm and 150 mm, suffered a single fracture at 125 mm, and multiple fractures at 100 mm and 50 mm. The smallest standoff distance resulted in the greatest number of fragments.

The main conclusion from this test program is that it is feasible to build in a 'throw away' load cell within the tibia bone of a modified FSL. The accuracy and repeatability of this built-in load cell will be less than for a high-precision metallic load, but it offers a practical alternative for tests with a high risk of damaging an anthropomorphic mannequin.

# Authors

**M.J. Footner**
Weapons Systems Division

*Michael Footner is a Senior Officer Technical who joined DSTO in 1975. He currently manages the WSD Rocket Motor Static Firing Facility and specialises in Transducers, Instrumentation and Data Acquisition. He has designed and supported FSL/FSLL/FSLM instrumentation since its inception.*

---

**D.M. Bergeron**
Weapons Systems Division

*Dr Denis Bergeron joined Defence R&D Canada (DRDC) Suffield in 1983. He was project scientist for DRDC research in mine neutralisation and mine effects from 1995 to July 2002 when he started a 2 year attachment with DSTO Edinburgh, where he is conducting research in mine protection and blast physics.*

---

**R.J. Swinton**
Weapons Systems Division

*Robert Swinton joined DSTO in 1967 and has specialised in explosive analysis, testing, sensitivity/hazard assessment, and device development. He is currently working in the Countermine Technology Group investigating landmine effects and associated countermeasures.*

---

# Contents

# 1. Introduction

## 1.1 Background

During the late 1990s, the Defence Science and Technology Organisation (DSTO) assembled a multidisciplinary team to develop an anatomically correct reproduction of the human leg. The Frangible Surrogate Leg (FSL) model, as it is called, is constructed around bones that are cast from a polymer composite while standard 'ballistic' gelatine is used to simulate soft tissues. A chamois material can also be added outside the model to simulate the skin.

Researchers in Australia and Canada have used the FSL in numerous tests to assess the performance of protective footwear against anti-personnel (AP) landmines. The FSL is an appropriate tool for this purpose given the destructive nature of such tests. The primary diagnostic is obtained from a post-test examination of the damage inflicted to the bones and soft tissues, which has often been performed by medical staff. The prognostic has usually ranged from simple dislocation to complete destruction of the lower portion of the model. This is useful to determine probable medical outcome, but post-test inspection of the FSL damage provides only part of the information. The time history of the load also provides insight into the damage mechanisms relating to landmine injury, as was demonstrated during Canadian tests [1] where a load cell had been introduced in the mid-section of the tibia. The load histories for FSL models that had been fitted with protective footwear were significantly different than when the FSL was fitted with a regular combat boot.

The FSL has also been used to assess the effect of anti-vehicular (AV) landmines on the occupants of land vehicles with and without protective measures. The FSL was often located near an anthropomorphic mannequin, such as the Hybrid III, that was equipped with a tibia load cell. In this manner, two complementary diagnostic methods were available to determine the probability of injury to the occupants. However, there are situations when important information would be missed if the mannequin is not used, but where the risk of damaging the lower extremities of the mannequin is high. In such a situation, mounting the FSL to the Hybrid III would be an attractive alternative, as long as the FSL can measure the load history. Another advantage of attaching the FSL to an anthropomorphic model of the human body is that it gives realistic boundary conditions for the inertial response of the FSL.

Introducing a commercial load cell in the tibia requires a significant level of effort. A segment of the bone first needs to be cut out, the load cell is then put in place with purpose-made adaptors, the upper and lower bones segments are aligned, and glue is finally used to bond the assembly together. Another disadvantage with inserting a commercial load cell in the bone is that it affects the propagation of the stress waves in the bone material because it is usually metallic. During the Canadian tests, artificial breaks were often observed at the interface where the load cell had been introduced.

Given these difficulties, it was proposed to cast a shortened tibia with a cylindrical section that could be instrumented with strain gauges. This built-in load cell could then be calibrated to measure both bending moments and compressive load. This work was carried out at DSTO in collaboration with Anatomical Surrogate Technologies Pty Ltd (AST) and Defence R&D Canada (DRDC).

## 1.2 The Modified FSL

The modifications to the FSL included shortening the length of the fibula and tibia bones by 95 mm and inserting a cylindrical section, 60 mm in length and 34 mm in diameter, in the tibia bone starting 190 mm from its distal end, as shown in the left specimens of Figure 1. This cylindrical section was instrumented with strain gauges to measure local bending and compression. The shorter fibula bone was attached to the same relative location under the proximal end of the tibia. The distal (lower) half of the FSLM is identical to previous versions of the FSL with the calcaneus and talus bones cast around porous inclusions to tune their failure response to that of real bones.

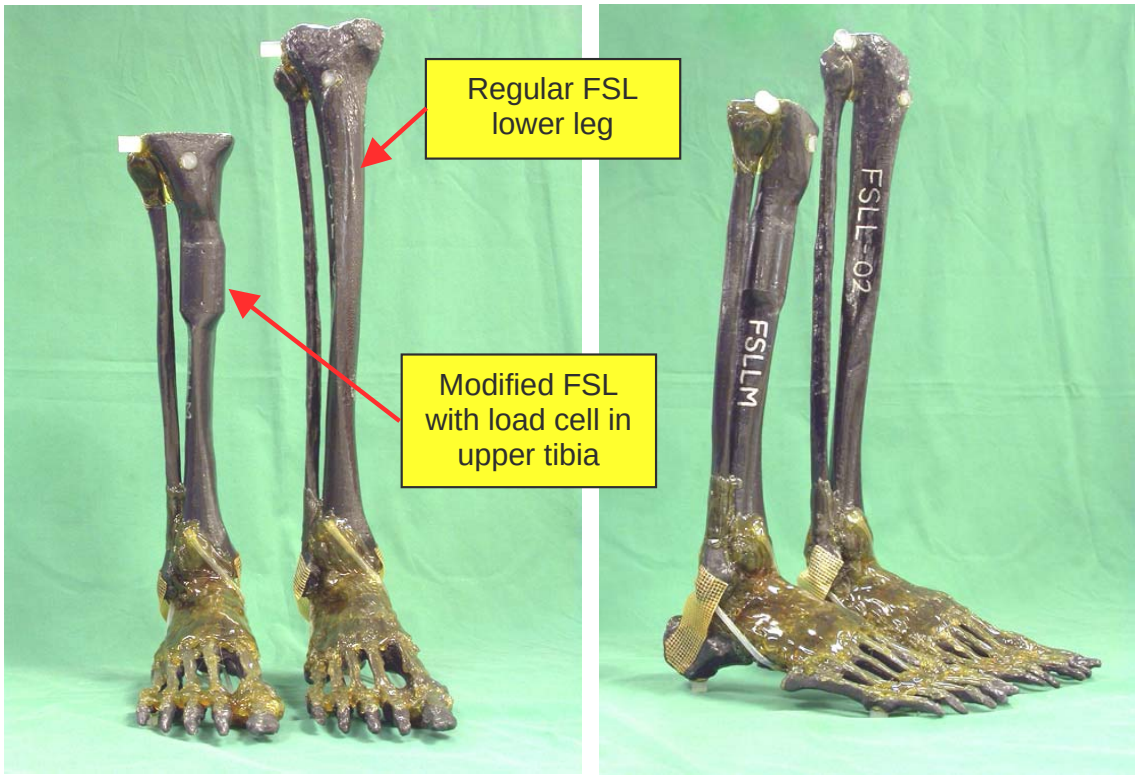


*Figure 1. Front view of the modified (left) and regular (right) FSL bones showing the placement of a circular load cell section in the upper part of the tibia. The lower halves are identical.*

The shorter length of the FSLM was selected for compatibility with the Hybrid III anthropomorphic mannequin. The flat end of the upper tibia makes it easy to mount the model on other devices as well. With the built-in load cell, it is now possible to

measure the time history of the stress flow through the upper section of the tibia bone. It should be noted that this stress flow is a function of the load process that takes place at the distal end of the FSLM, which is a function of the failure mechanisms [2] that take place in the calcaneus and talus bones at the lower end of the model.

### 1.3 Objectives of the Present Work

The first portion of this report presents a summary of the work done to calibrate the modified Frangible Surrogate Leg (FSLM). However, once the calibration process was completed, it was decided to subject the instrumented legs to varying explosive loads and to document the response of the FSLM. Thus, there were two clear objectives to the present work as follows:

1. Using non-destructive techniques, develop simple calibration equations for the compression force and the bending moments measured by the instrumented FSLM. Examine the accuracy of the equation for compression force from test to test as well as from one model to the next.

2. Measure the response of the instrumented FSLM to varying explosive inputs representative of an AP landmine. The approach taken to vary the explosive force was to use the same explosive charge, consisting of 50 grams of PE4 buried under 20 mm of sand, and vary the height of the FSLM above this charge.

## 2. Calibration and Explosive Test Procedures

### 2.1 Strain Gauge Instrumentation of the FSLM

A specific arrangement of the strain gauges is required to differentiate between compressive strain and strain due to bending. Geometric symmetry in the strain measurement region is essential. It makes it possible to place the gauges and connect the electrical bridge such that strain induced by an unwanted input can be cancelled out. Using this principle, meaningful measurements can be achieved. It is even likely that the accuracy can approach that of more expensive load cells.

The strain gauges selected for the current application were Micro-Measurement CEA-06-125UT-350. These were bonded to the FSLM with M-Bond 200 adhesive. Given the experimental nature of the current tests, it was decided to place four strain gauges, each 90° apart, about the cylindrical section, as shown in Figure 2. All strain gauges measured strain in the axial direction, i.e., along the length of the bone. Opposite strain gauges were aligned so that one pair would point in fore/aft direction while the other pair pointed in the inside/outside direction, which corresponded to the left/right sides of the body. Accurate placement was aided by the incorporation of alignment markers machined into the casting mould dies for the tibia. Looking down onto the top of the

right leg model, the gauge locations were front (SGFA), back (SGBA), inside (SGIA) and outside (SGOA). The wiring diagram for these strain gauges is given in Appendix A. This diagram includes four transverse strain gauges. These are usually used for temperature compensation. Although these signal were recorded during the current tests, they did not provide additional information above that obtained from the axial gauges, hence data from these transverse gauges will not be discussed any further.

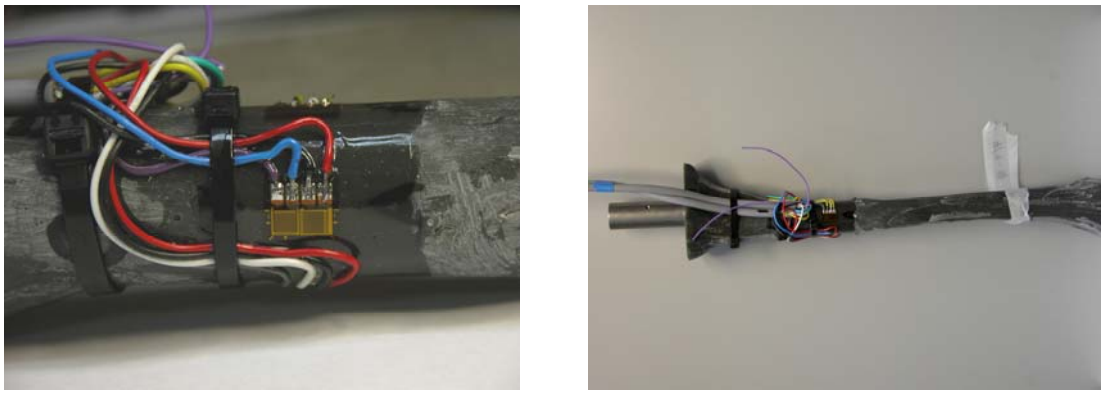

*Figure 2. Four strain gauges were placed at equal intervals around the cylindrical section of the upper tibia.*

By recording the signal from individual strain gauges, it was possible to compute two compression load histories and two bending moments when post-processing the data. Adding the individual signals from opposite strain gauges cancels out the contribution from bending, leaving a pure compression signal. Conversely, subtracting these two same signals cancels out the contribution due to compression, leaving a pure bending signal. Thus, four channels of data were derived as described in Table 1.

*Table 1. Post-processing of individual strain gauge signals to compute pure compression and pure bending moments.*

| Derived Channel Description | Channel Name | Manipulation |
|---|---|---|
| Axial Compression 1 | C1FBA | SGFA + SGBA |
| Axial Compression 2 | C2IOA | SGIA + SGOA |
| Bending Moment about X axis | Mx | SGIA - SGOA |
| Bending Moment about Y axis | My | SGFA – SGBA |

## 2.2 Experimental Apparatus

Figure 3 shows the test rig used for these tests. The rig consisted of a soil container with two vertical beams on opposite sides of the container and a horizontal crossbeam that was free to slide up and down the vertical beams. A single axis reference load cell, calibrated to 25 kN, was attached to the centre of the crossbeam. Each FSLM model, fitted with a regular combat boot, was attached to the load cell using a 20 mm diameter steel pin that was glued to the top of the FSLM. The initial height of the boot above the

soil was adjusted by placing wooden stops at the base of the rails on each side of the container. The total mass of the crossbeam, FSLM, and footwear, was approximately 27 kg. A Celesco MTA2-30E-33-10k-C1 cable-pull transducer was attached to one side of the rig to measure the vertical displacement of the crossbeam.

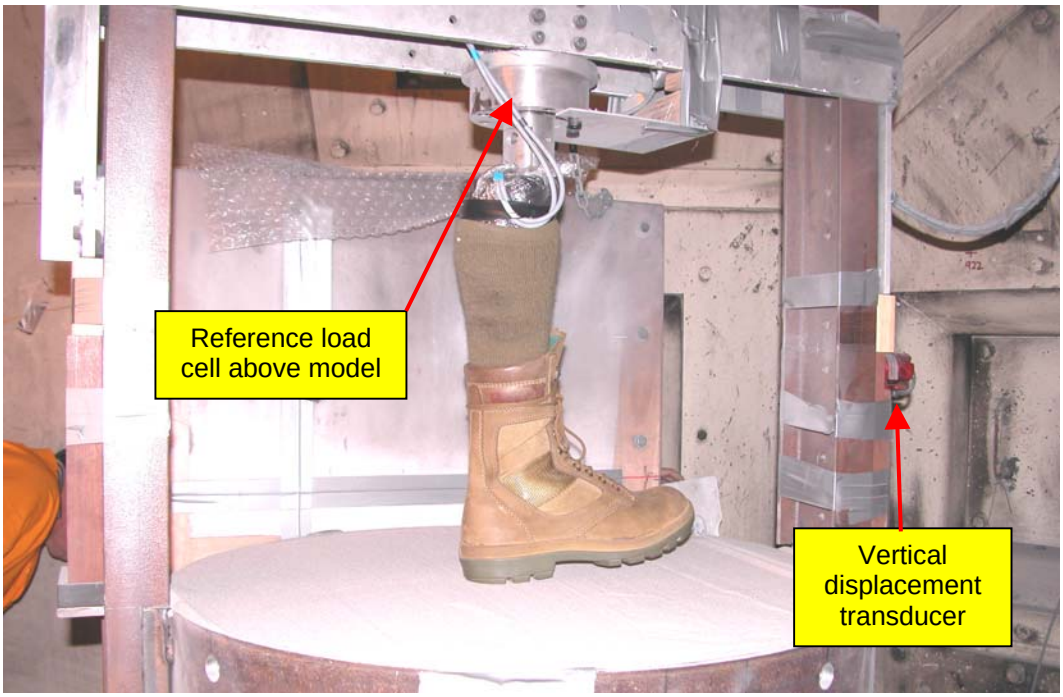


*Figure 3. The FSLM was attached to the crossbeam of the test rig through a reference load cell. A cable transducer measured the vertical displacement of the crossbeam.*

## 2.3 Calibration Procedures

Different procedures were used to calibrate bending moment and compression force. A coarse calibration of the bending moments was done using static loads while a dynamic method (drop tests) was used to calibrate the strain gauge outputs against the vertical load measured by the reference load cell.

### 2.3.1 Static Calibration of Bending Moments

An approximate calibration of the bending moments was performed only for the $x$ and $y$ axes. For this work, the axes were defined relative to the generally accepted convention for the human body. The $x$-axis pointed in the forward direction while the $y$-axis pointed to the right hand side of the body. Applying the right hand rule for vectors, this meant that the $z$-axis pointed in the downward direction. The calibration procedure was repeated for each FSLM along two mutually perpendicular directions, as depicted in Figure 4. Each models was attached to the crossbeam at a height such that the bottom of the boot was above the side of the container. A string was wrapped

around the lower end of the FSLM/boot combination and a force was applied along the horizontal plane. A simple spring balance was used to measure the applied load. Once the load was stable, the strain gauge data was recorded for a short period of time.

*Figure 4. Technique used to apply static bending loads to the FSLM models.*

Appendix B presents a summary of the calibration data. The applied moments ranged from 3.92 to 15.69 N-m. It was decided to limit the calibration to this relatively small range given that the FSLM deflection was becoming significant. A linear best fit to the data from the five FSLM models yielded the following 'generic' calibration formulae.

$$M_x = 55.768\varepsilon - 8.7914 \quad ; \quad R^2 = 0.9846$$
$$M_y = 118.58\varepsilon - 6.1595 \quad ; \quad R^2 = 0.9951$$

where $\varepsilon$ is the microstrain.

### 2.3.2 Dynamic Calibration of Compression

Given the availability of the reference load cell, it was decided to use a dynamic technique to calibrate the strain gauge response under compressive loading. The technique simply consisted of dropping each FSLM/boot combination several times from a preset height of 200 mm. One FSLM was dropped from 300 mm, but this caused a dislocation of the ankle joint and the height was reduced thereafter. The boot was impacting against a hard steel surface constructed from steel blocks mounted atop bricks placed in the soil container. The latter had been emptied for these tests.

It should be noted that the FSLM construction technique yields a semi-rigid leg. When the model was mounted vertically in the test rig, the foot did not rest flat on the ground, as shown in Figure 5. The toes were slightly elevated, which corresponded to the heel-strike phase of walking. It is also important to note that the heel was not fully parallel to the ground in the lateral direction either. These offsets of the contact point relative to the long axis of the leg, and the fact that the bones of the leg are not truly vertical, meant that each drop automatically produced a bending moment.

*Figure 5. Position of the boot is not flat due to design of the FSLM model.*

## 2.4 FSLM Response to Explosive Loads

The FSLM was subjected to five explosions in order to assess its response to varying explosive inputs. In the present context, the word *response* refers mainly to the strain gauge signals and the damage inflicted on the composite bones. This required detailed procedures as follows.

### 2.4.1 Explosive Test Procedure

The procedure for the explosive tests was carried out in accordance with the guidelines of a NATO task group [3] that had examined how to test footwear against the effects of anti-personnel landmines. The explosive charges consisted of 50 grams of plastic explosive (PE4) packed in a short cylindrical container with an internal diameter of 49 mm and an internal height of 17 mm. These containers were made of plastic and had a wall thickness of 1.5 mm. The charges were detonated with a RP-501 electric bridge wire detonator placed a bottom dead centre.

The explosive charges were buried in dry sand with particle diameter between 300 and 700 microns. The sand was simply poured in the steel container that was 800 mm in diameter and 500 mm deep, and then levelled with the top rim of the container. The surface of the soil was then used as a datum for the depth of burial of the explosive charge and the standoff distance of the footwear. The charges were buried in the centre of the container, which was determined by crossing perpendicular lines. This point was also vertically below the central axis of the load cell. The top of the charge was located 20 mm below the soil surface.

### 2.4.2 Variation of the Explosive Load

In order to vary the strength of the explosive input into the FSLM model in a controlled and consistent manner, it was decided to always use the same explosive charge and

burial method, but to vary the height of the model above the charge. This technique had been used successfully in Canada in the past [4]. The intent was to produce varying levels of damage to the calcaneus bone, from no break to severe disintegration. The first test at a height of 200 mm resulted in an intact calcaneus (there was however damage to the foot), hence all subsequent tests were carried out at smaller standoff distances as follows: 150 mm, 125 mm, 100 mm, and 50 mm. This produced a wide range of damage levels to the calcaneus.

### 2.4.3 Flash X-Ray Set-Up

The flash radiography set-up depicted in Figure 6 was used during the explosive tests. Two x-ray units, A and C, were placed at a 45° angle to each other such that the centre of their beams intersected on the centreline of the soil container. The centre of the beams was 50 mm above the soil surface. The source-to-target distance was 2,500 mm and the source-to-film distance was 3,040 mm, which gave a magnification factor of 1.216X. A purpose-build cassette was used to minimize the lateral separation between the x-ray films. Horizontal and vertical fiducial lines were placed on the outer face of the film cassette to generate visual reference marks on the films. For each test, four radiographs were produced. A static exposure was taken from each x-ray unit just prior to the test. Exposures were then taken from unit A at 1 ms after detonation, and from unit C at 2 ms.

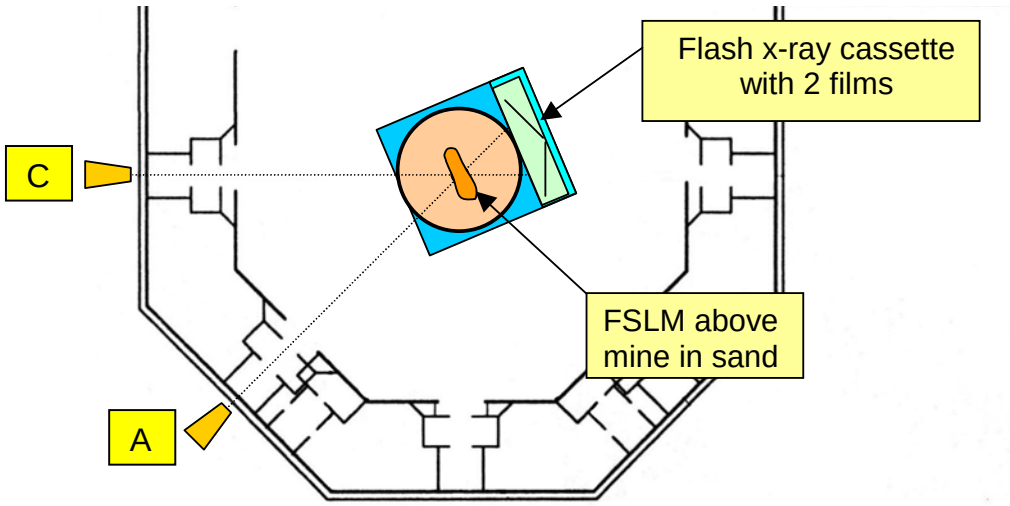


*Figure 6. Plan view of the flash radiography set-up used for the explosive tests.*

### 2.4.4 Analysis of the Flash X-Ray Images

The flash radiographs were analysed to determine the motion of a steel insert (see Figure 7) within the sole of the footwear and to assess the progression of bone damage in the leg model. However, because the FSLM is a non-symmetric three-dimensional


*Figure 7. The motion of the metal insert in the sole of the boot was analysed.*

object, the two x-ray heads produced different views of the leg. The A head generated a slightly frontal view of the leg that clearly showed the separation between the tibia and fibula bones. The C head looked at the leg slightly from the rear with the fibula being in front of the tibia; hence the fibula cannot be clearly differentiated from the tibia. It should be noted that for most people, these subtle differences in the two views are noticeable only when overlaying the radiographs.

Nevertheless, the images were sufficiently similar that an accurate analysis of vertical motion could be performed provided static images from each x-ray unit were available. These static images provided the reference required to determine the horizontal and vertical displacements. A detailed analysis of bone motion, as presented in Reference [2], was not performed. The bone damage data sought in the present study was obtained only from the post-test examination of the boot/leg model remains.

### 2.4.5 Physical Inspection of Footwear and FSLM Models

A physical inspection procedure was used to document the extent of damage to each FSLM and to the footwear. At the completion of each test, the following steps were followed in the order listed:

- The state of the test set-up was documented with digital photography.
- The boot remains and FSLM were removed from the test chamber.
- The floor was swept and the sand was sieved to find fragments of boot, bone and gelatine.
- The major portion of the FSLM was examined, with the boot still attached, to assess the extent of fractures to the FSLM bones.
- The boot and sock were removed and the damage to them was assessed and documented.
- The altered FSLM models were sent to Anatomical Surrogate Technologies Pty Ltd for a supplementary assessment of the damage.
- Later on, each FSLM was debrided of its ballistic gelatine to extract the bones.
- The bones were re-assembled, photographed, inspected, and the damage was documented.

# 3. Results from the Drop Tests

The drop tests provided the data necessary to establish a calibration of the compression force for the FSLM strain gauges. Figure 8 is a plot of the vertical height of the boot above the hard surface overlaid with the load cell signal, which reveals the dynamics of a typical drop. In this particular instance, it took 235 ms for the FSLM to accelerate and cover the 200 mm drop distance. The displacement appeared to 'penetrate' the steel as the rubber sole of the boot compressed and stored sufficient energy for the FSLM to rebound to a height of 20 mm. A second impact occurred 130 ms later and the FSLM finally came to rest about 550 ms after the beginning of the drop test.

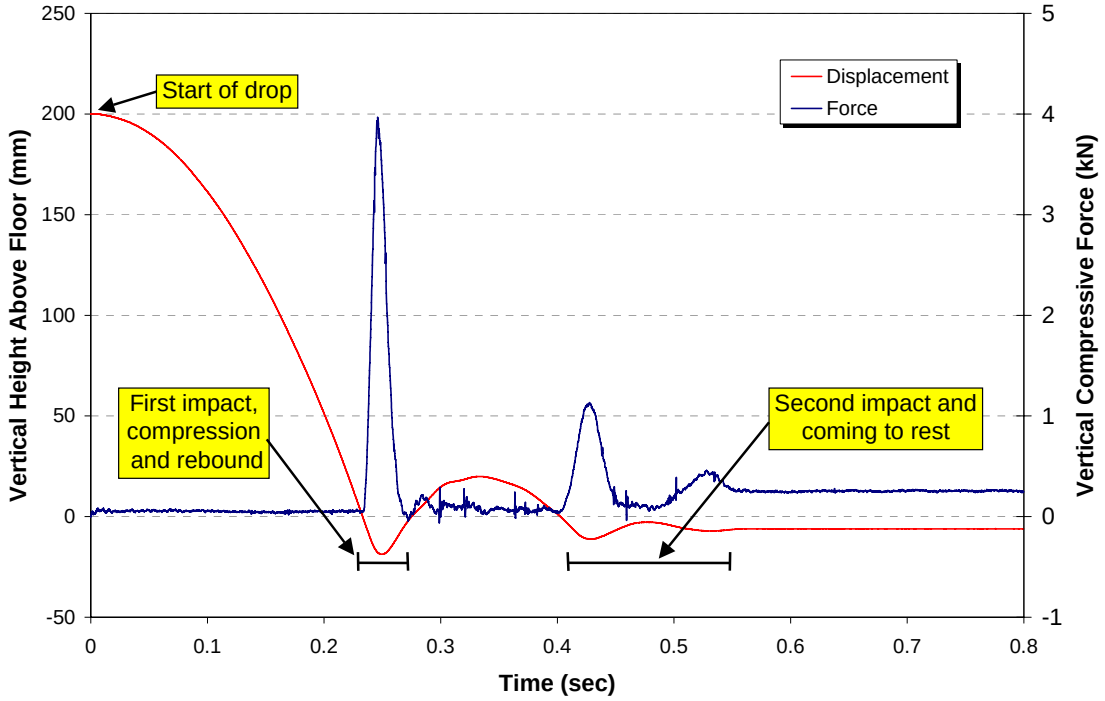


*Figure 8. Overlay of displacement and load cell traces for a drop test.*

Two factors affected the peak force measured with the load cell. These were impact velocity and the footwear fitted to the leg model. The impact velocity depended primarily on the height of the drop, but the sliding friction of the crossbeam also affected it. Reference [2] described how it was necessary to pay close attention to the cleanliness of the linear bearings and the mass balance of the crossbeam in order to minimise variations of the sliding friction. For some drop tests, friction decreased the impact velocity, which lowered the rise rate of force and resulted in a lower peak force.

The choice of footwear also had a strong effect on the peak force. This was noticeable when using a new versus an old boot. The new boots had thicker soles and more supple rubber, thus providing more cushioning and resulting in a lower peak force.

This section explains the methodology employed to determine the calibration equation for compression and examines the variation of the response of a given leg from test to test. Variations from one leg to another are also examined.

## 3.1 Calibration Methodology

The basic premise behind the drop test technique was that the system (Boot + FSLM + load cell + crossbeam) would respond such that the load cell and strain gauge traces would have the same functional form. This was possible because the load resulting from the drop increased at a rate that was much lower than the speed of sound in the FSLM bones structure. Thus, the whole system was considered to be in a state of quasi-static equilibrium at any given time. Figure 9 shows an overlay of the strain gauge and reference load cell responses (on different vertical scales) that clearly demonstrated the validity of the quasi-static equilibrium assumption for the drop tests.

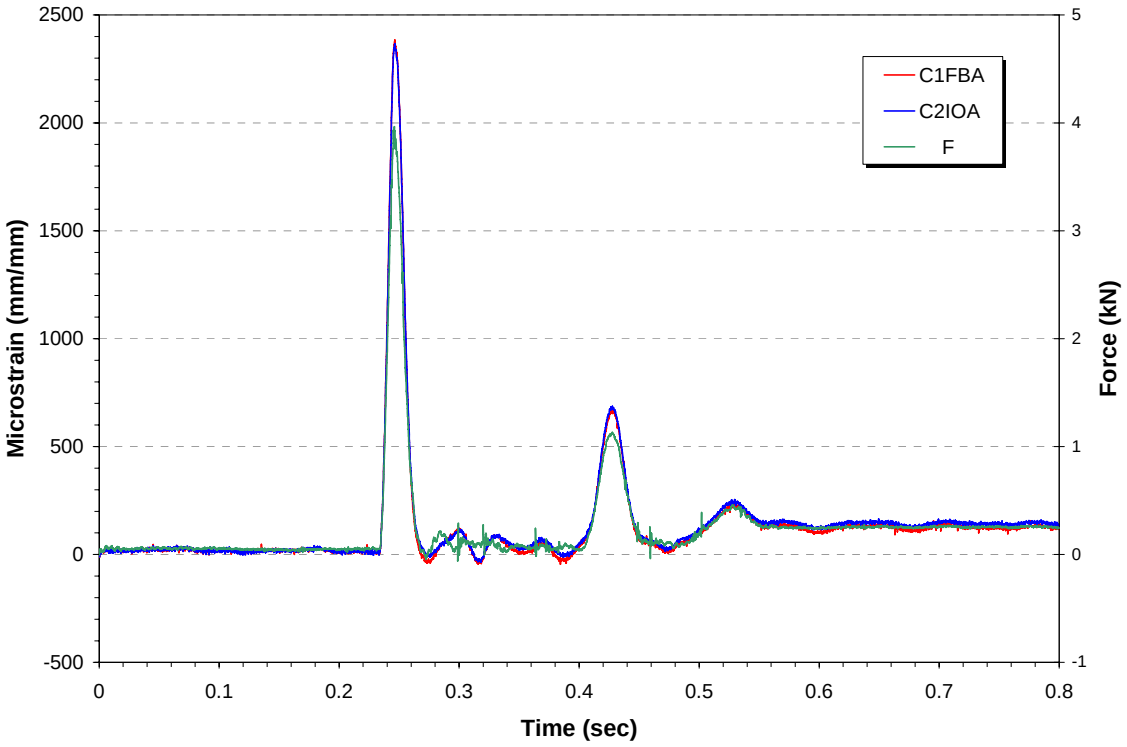


*Figure 9. Overlay of the strain gauges and load cell traces for a 200 mm drop test.*

The load cell and strain gauge data were recorded at 50,000 samples per second. For a 200 mm drop, all three traces started to rise at 236 ms and peaked 12 ms later. The slope of all curves increased gradually during the first 2 ms, remained constant for the next 8 ms, and progressively decreased back to zero over the last 2 ms. The maximum slope was $2.49\times10^{5}$ $sec^{-1}$ for strain and 436 kN/sec for the load.

Given that the system was in quasi-equilibrium, it was possible to extract points from the three curves that corresponded to the same time. This process could have been done for the entire rise time history, but it was instead decided to extract points only at those times that corresponded to 0.5 kN increments along the load curve. For a 200 mm drop, this usually yielded seven points from 0.5 to 3.5 kN, which was a manageable, yet sufficient, number of points for the purposes of calibration.

## 3.2 Variation from Drop to Drop for a Given Leg

Annex C presents the results for all drop tests carried out with the five FSLM models. *Figure 10* shows the results for FSLM#1, channel C1FBA, for three consecutive drops. For this low load regime, the linearity of the data for individual drops was very good, as indicated by the goodness of fit ($R^2$) values that ranged from 0.9955 to 0.9998 for all tests with all the models. The example below shows that the slope and offset varied from one drop to the next. The slope of the linear curve fits ranged from 1.540 to 1.654 Newton/microstrain, representing a 7.2% variation relative to the average slope, 1.581 Newton/microstrain. It should be noted that the results for FSLM#1 displayed the worst variation of the five legs. The best results were obtained for FSLM#4 with the three tests producing slopes that were within 1% of the average, thus showing excellent repeatability from test to test.

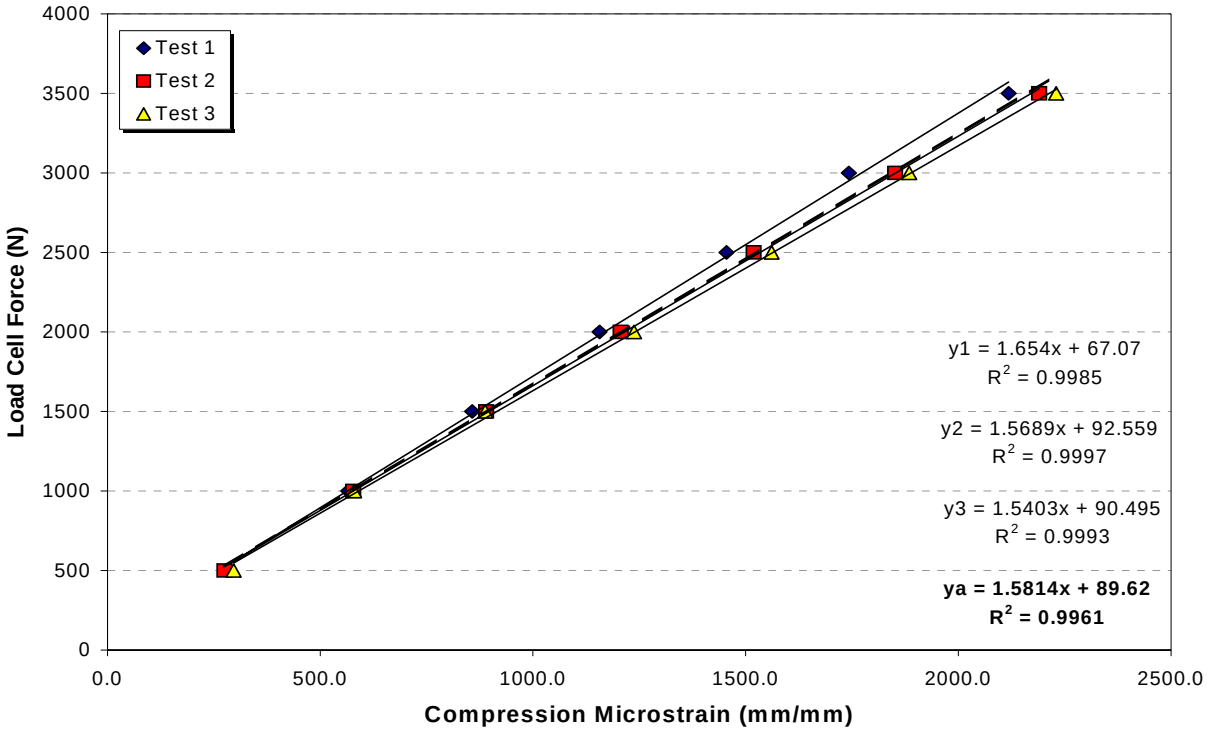


*Figure 10. Typical dataset used to derive the calibration equations for compression force.*

Table 2 lists the slopes for the first three drops with each leg. It is seen that the slope for the first drop was greater than for subsequent drops. It was also noted that the change in slope generally decreased from one drop to the next, suggesting that it was converging to some final value. Close inspection of the data in Annex C will reveal that FSLM#2 was dropped six times from 200 mm. This leg was the first to be tested and was therefore used to fine tune the test procedure. The reader will note that the slope decreased progressively for the first four drops, but increased suddenly at the fifth drop. This occurred after changing from a new boot to and old boot. The result demonstrated the capacity of the instrumented FSLM to detect changes in footwear configuration.

*Table 2. Slopes for the first three drops of the five leg models, channel C1FBA.*

| Drop No | FSLM#1 | FSLM#2 | FSLM#3 | FSLM#4 | FSLM#5 |
|---|---|---|---|---|---|
| 1 | 1.6540 | 1.4519 | 1.5797 | 1.5492 | 1.5632 |
| 2 | 1.5689 | 1.3692 | 1.5390 | 1.5387 | 1.4916 |
| 3 | 1.5403 | 1.3788 | 1.5367 | 1.5358 | 1.4712 |

The change in slope listed in Table 2 occurred according to a certain pattern. What was the underlying reason? This question requires careful consideration of the load path and the factors affecting it. But first, it is important to understand what the gradual shift in slope means. The slope is expressed in Newton/microstrain. When the slope decreased, it meant that for a given load reaching the reference load cell, there was more deformation sensed by the strain gauges bonded to the bone. If we assume that the physical and mechanical properties of the bone material did not change appreciably from one drop to the next, then it means that more of the load was transmitted through the tibia.

The above statement should be considered from the point of view that the load cell built into the tibia measured only a portion of the overall load that was being transmitted to the reference load cell. It is generally accepted that the tibia is the main load carrying bone. However, since the fibula is physically attached to the distal and proximal ends of the tibia, it provides an alternate load path around the load cell portion of the tibia. The shift in slope indicates that a redistribution of the load between these two bones occurred. It is therefore suspected that the change in slope was due to minor breaks of the glue joints of the FSLM during the first drop. This made it more difficult for the fibula to carry as much load to the reference load cell.

The 'softening' of the glue joints might also have affected how the load was transmitted through the bones before reaching the reference load cell. Thus, for the same load being applied to the bottom of the leg, the sole of the foot might have caused a rotation of the calcaneus, which introduced a small time delay in transmitting the full vertical load to the talus and then to the tibia and fibula bones. Compression at each joint introduced a similar time delay in the load transmission. These time delays ultimately reduced the peak force measured by the reference load cell.

### 3.3 Variation Between Channels and From Leg to Leg

The variations of the response between channels on a given leg and from one leg to the next were assessed by comparing the average slope for the two compression channels of all five legs, as listed in Table 3. For a given leg, the difference between channels ranged from less than 1% up to 7% relative to the average slope for the two channels. This is relatively good. However, the variation from one leg to the next was significant. The worst case is for channel C2IOA between legs #2 and #3, which is 17.7% relative to the average for the channel. These results provide a rough estimate of the accuracy and repeatability of the load cell built into the FSLM. It can be said that an overall accuracy of the order of 15% is to be expected. This number holds true for low strain rate, and further work would be required to assess the accuracy of the built-in load cell at high strain rate.

*Table 3. Summary of the average slopes for the five leg models.*

| Channel | FSLM#1 | FSLM#2 | FSLM#3 | FSLM#4 | FSLM#5 | Average | St Dev |
|---|---|---|---|---|---|---|---|
| C1FBA | 1.581 | 1.415 | 1.568 | 1.540 | 1.506 | 1.522 | 0.067 |
| C2IOA | 1.604 | 1.405 | 1.682 | 1.587 | 1.541 | 1.564 | 0.102 |

# 4. Results from the Explosive Tests

The results of the explosive tests were examined through the reduction of data from three different sources. First, the flash x-rays taken at 1 and 2 ms after detonation provided a visual record of the damage process that took place during the experiments. By comparing these x-ray images to two other images taken immediately before the test, it was possible to track the position of the steel insert, which was in the sole of each boot, and to approximate its velocity. Visual inspection of the physical damage to the boots and to the FSLM provided the second source of data. Finally, the third source of data was the time histories of the reference load cell and the four strain gauges on the tibia of the FSLM.

### 4.1 Description of the Overall Event

The flash x-ray diagnostic provided insight into the damage processes that occurred to the FSLM during the explosion. Figure 11 shows three x-rays for each test, which correspond to immediately before the explosion (head A only), 1 ms after detonation, and 2 ms after detonation. Given that the position of the x-ray film cassette was never changed during the test series, the standoff from 50 mm to 200 mm is easily deduced from the location of the FSLM in the picture.

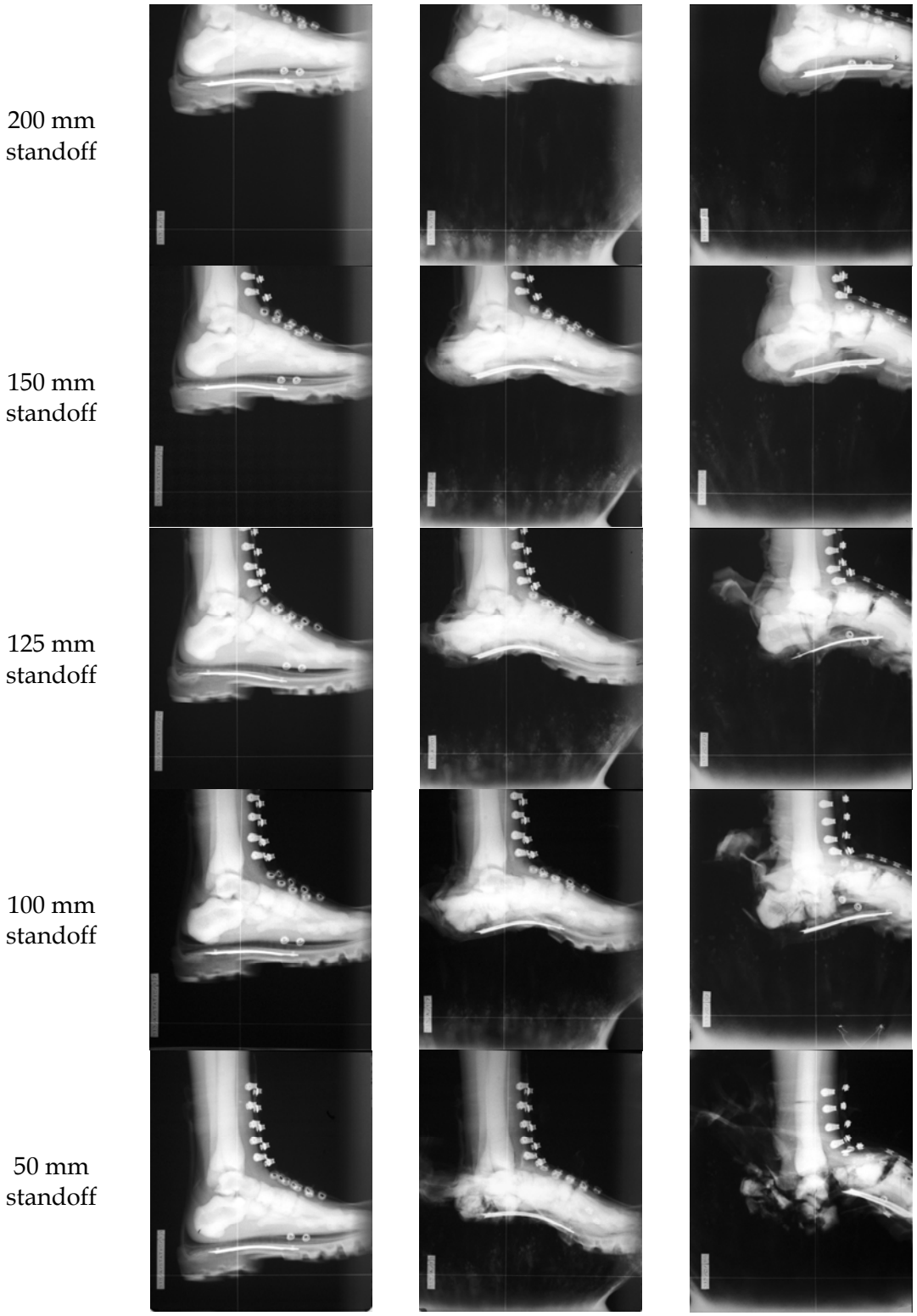


*Figure 11. Flash x-ray pictures for various standoffs against 50 grams of plastic explosive buried below 20 mm of sand: left = 0 ms, centre = 1 ms, and right = 2 ms.*

Standoff influenced the rate of development of the damage. Thus, by comparing the five pictures at the same time, 1 ms or 2 ms, it is immediately apparent (as expected) that damage occurs at a faster rate for smaller standoff distances. The pictures also show that the severity of the damage increased when the FSLM was located closer to the explosive charge.

For 50 mm, 100 mm and 125 mm standoffs, there was severe fracturing of the calcaneus and talus within the first millisecond after the explosion. Dislocation of the fore foot was also visible in all cases. For the smaller standoff distances, the front of the foot actually sheared off ahead of the talus due to the push of the explosion against the large surface area of the fore foot ahead of the tibia and fibula.

By comparing each static exposure to the corresponding x-ray image at 1 ms, it was easy to see how the explosion pushed the sole of the boot in the upward direction. The curvature of the spring steel insert increased appreciably for standoff values of 150 mm and less. It is also seen that the spring steel had straightened back by 2 ms in all cases. In several pictures, there was a change in the aspect of the spring steel insert, which indicated a rotation about its long axis. The sole of the boot also appeared to rotate relative to the foot. This rotation could also have been the result of strong bending of the whole leg about its upper attachment point to the crossbeam of the test rig

## 4.2 Flash X-Ray Results and Analysis

The position of the spring steel insert provided an excellent diagnostic to measure the strength of the explosive force transmitted to the boot and FSLM model. A greater velocity indicated that a greater force had been transmitted. Hence, the position of each steel insert was measured using three points located at each extremity, and one point selected near the centre arbitrarily from visual inspection. The coordinates are accurate to within 1 mm. The displacement of each insert was determined by shifting the position of the rear (leftmost) point for the static A and C radiographs to a zero-zero origin. All other points were then shifted by the same amount to obtain a measure of the relative displacement of the steel insert at each standoff distance. The results are plotted in Figure 12.

Two observations are apparent from this method of presenting the data. First, it is seen that the initial position of the steel insert changed from one test to the next, particularly with respect to its angle relative to the horizontal. This might have been due to slight variations in how the boot was fitted to the FSLM from test to test. The second observation relates to the curvature of the insert at 1 ms after detonation and its rapid recovery within the next millisecond. It is important to note that the recovery was along the front portion of the insert as it penetrated the gelatine in the mid-foot region. The rear portion of the insert was pushing against the base of the calcaneus, and thus against the talus and long bones, which offered more resistance to upward movement. For the 50 mm case, the insert was expelled forward when the front portion of the foot was completely severed from the long bones after the ankle bones had disintegrated.

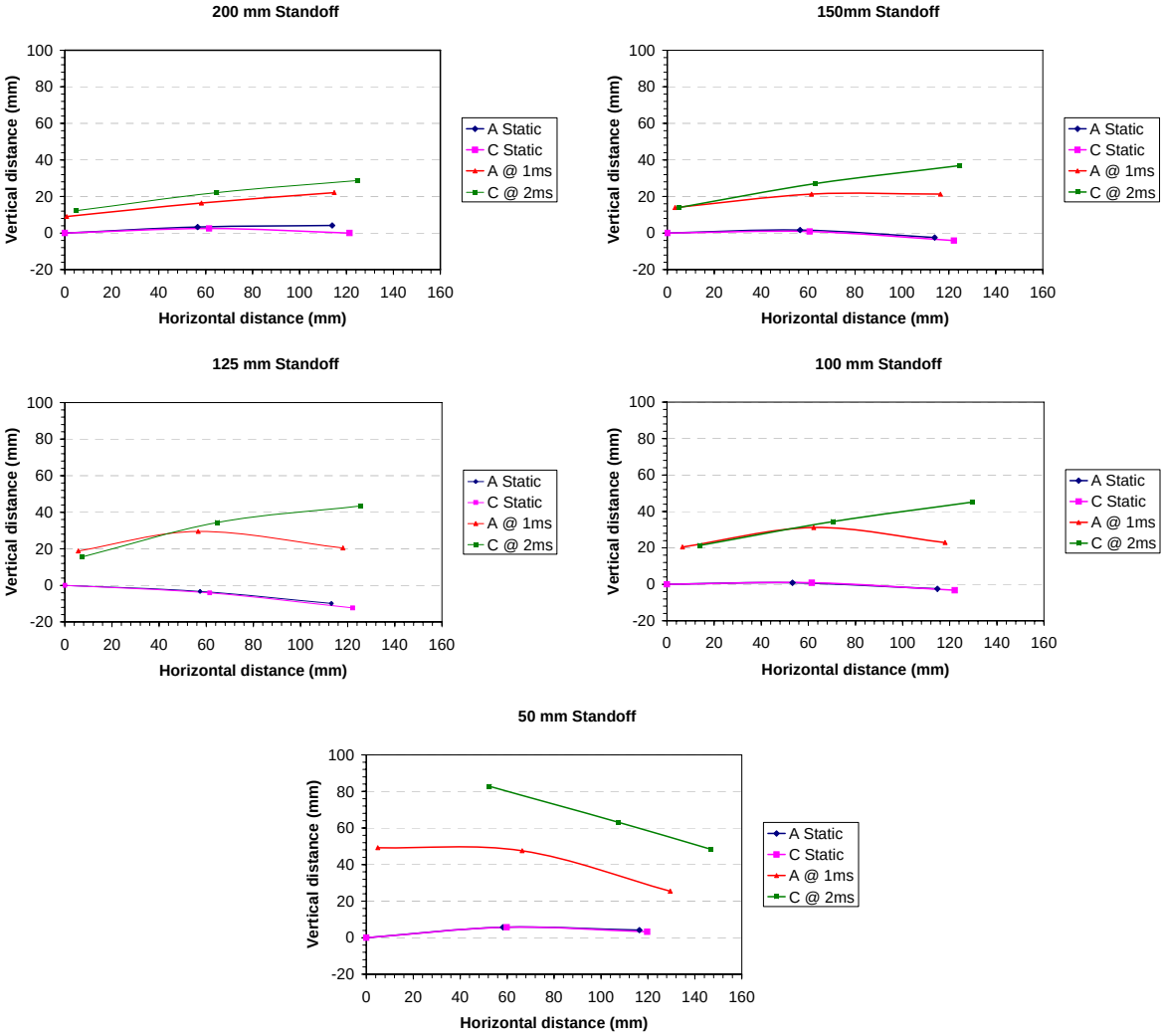


*Figure 12. Displacement of the steel insert in the boots at 1 and 2 ms versus standoff.*

The average velocity of the insert was approximated from the displacement data. Since the mid-point position varied from one x-ray to the next, it was decided to fit a straight-line segment between the end points and use the displacement of the centre for each case. An average velocity was then computed by dividing this centre point displacement by the time. Figure 13 shows a plot of the results. In all cases, except for the 50 mm standoff, the centre point velocity is higher during the first millisecond after detonation. The different behaviour observed for the 50 mm case reflects the change in the damage mechanism when the front of the foot was severed. From the data, it is seen that the velocity decreased steadily as standoff was increased, suggesting (as expected) that it would have reached zero when the standoff would have become very large.

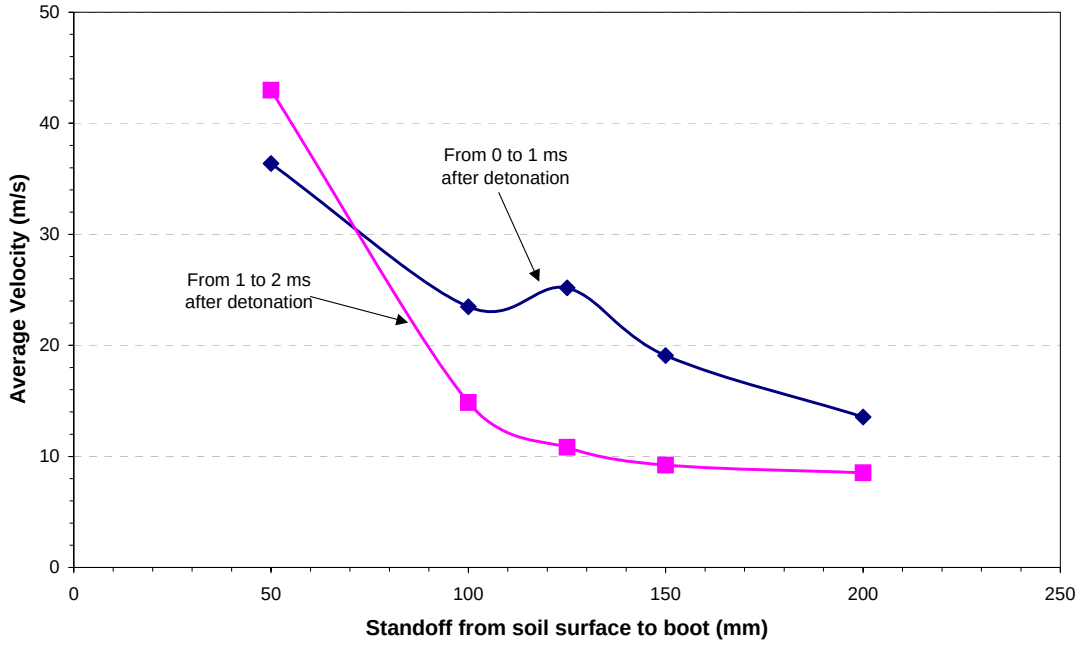


*Figure 13. Average velocity of the steel insert for the 1st and 2nd millisecond versus standoff.*

## 4.3 Damage to the Combat Boots

The damage to the combat boots increased significantly as the standoff was reduced from 200 mm down to 50 mm. Furthermore, the severity of the damage correlated well with standoff distance. Annex D provides pictures and a description for each test. At 200 mm, there was only superficial damage to the exterior of the boot due to abrasion and overstressing of the rubber material. The structural integrity of the boot was preserved, thereby preventing the ingress of contaminants. This was not the case for the smallest standoff distance (50 mm) which resulted in complete disintegration of the rear portion of the boot. This exposed the FSLMs soft tissues and lower bones to the flow of dust and soot.

The boot damage at 150 mm was also superficial, consisting of abrasion and minor tears of the rubber sole. There was, however, more damage to the inner sole due to its strong impact with the bottom portion of the calcaneus bone, all of which left a permanent imprint. Reducing the standoff distance by only 25 mm, down to 125 mm, was sufficient to cause major tears of the rear portion of the rubber sole and the separation of some fragments. Many of the large fragments were also pushed into the lower part of the FSLM and allowed the ingress of contaminants. Similar results were observed at a 100 mm standoff, except that the damage was noticeably more severe.

## 4.4 Damage to the FSLM Bones

The physical damage to the FSLM specimens was examined in three stages. First, an examination was carried out immediately after the test and recorded with digital photography. Gelatine was partially removed during this stage to provide better access to the bones. The second stage was an off-site examination performed by the staff of Anatomical Surrogate Technologies Pty Ltd. For the third stage, the gelatine was removed completely from the specimens and the remaining bones were photographed to provide a visual record of the level of damage as a function of standoff. This photographic record is shown in Figure 14 while Annex D provides a description.

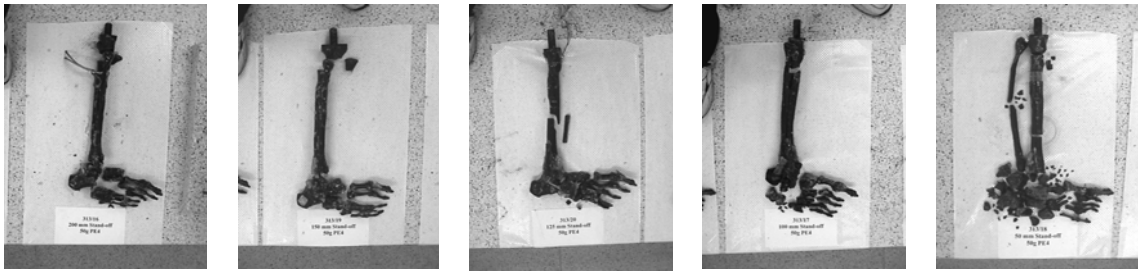

*Figure 14. Increasing damage to the FSLM bones with decreasing standoff, as seen from the size and number of fragments above; standoff from left to right: 200, 150, 125, 100, and 50 mm.*

The effect of standoff could easily be quantified from the severity of bone fractures to the calcaneus, talus, bones of the mid-foot, and the long bones. For a 200 mm standoff, the calcaneus, talus and fibula bones were intact. There was a proximal fracture of the tibia near its attachment point to the test rig, but it was assessed that this fracture was an artefact of the test model, as it did not correlate with results from tests against cadavers that were performed in the United States [5]. Although the damage to most bones was minimal, the bones of the mid-foot suffered multiple dislocations and a limited number of fractures. This is attributed to the large surface area that the foot presents to the mine blast flow ahead of the long bones. The push of the flow on the calcaneus and talus is resisted by the long bones, but there is nothing to resist the force on the bones of the mid-foot, which underwent large deformation leading to the damage that was observed. It should be noted that the bones of the mid-foot were damaged during each test, but the severity and number of fractures increased as the standoff distance was reduced.

As the standoff distance was gradually reduced, the severity of the bone fracture patterns increased. This was particularly noticeable with the calcaneus, which suffered no damage at 200 mm and 150 mm, and exhibited a single fracture at 125 mm. At 100 mm, there were multiple fractures that produced several large fragments. At 50 mm, the calcaneus fractured into a significantly greater number of smaller fragments.

A similar pattern was observed for the talus bone, which was either intact of suffered dislocation near its front end for standoff distances of 200 mm, 150 mm and 125 mm.

At 100 mm, the talus fractured into several large fragments. At 50 mm, it was reduced to multiple small fragments.

Damage to the long bones could also be used as a metric if fractures above the mid-length were neglected. This recognizes that bone damage above the mid-length was affected by both the introduction of the load cell, and the FSLM's attachment to the test rig. Thus, using this criterion, the tibia and fibula were intact at standoff distances of 200 mm, 150 mm, and 100 mm. At 125 mm and 50 mm, there were mid-shaft and lower one-third-shaft fractures of both bones. The fact that the long bones were damaged at 125 mm, but not at 100 mm standoff, might be related to the initial position of the leg in the test rig, as indicated by the inclination of the spring steel insert in the sole of the boot (shown in Figure 12). This might suggest that long bone breakages are more a function of the bending moment associated with misalignment of the leg model's long axis, and the load vector. The talus and calcaneus bones produced damage that was more consistent with the load conditions; the authors had greater confidence in the results from these bones, as reported from Canadian experience [4].

## 4.5 Response of the FSLM Strain Gauge Instrumentation

The reference load cell and the strain gauges performed reliably throughout the test series, which provided the information needed to assess how well the load cell built into the FSLM bone worked under high strain rate conditions. The upper plots of Annex E present the loads that were recorded directly from the reference load cell and computed from the strain gauges. The lower plots present the corresponding bending moments that were computed from the strain gauges.

Figure 15 consists of two plots of the vertical load signals in the vicinity of the peak force for the 200 mm (left) and 50 mm (right) standoff distances. The general trends for these two standoff distances are discussed first. It is clearly evident that the magnitude of all signals correlated well with the standoff distance. The maximum amplitude of the reference load for the 200 mm standoff was 13.2 kN, which was 3.3 times less than the 43.4 kN peak load measured for the 50 mm standoff. This is consistent with practical experience and intuition, i.e., that the load transferred to an object is greater when the object is closer to the explosion. Another aspect of these signals is that the peak load was reached 0.74 ms after detonation for the 50 mm standoff, while it was reached at 1.13 ms for the 200 mm standoff. This is also consistent with the physics of the problem.

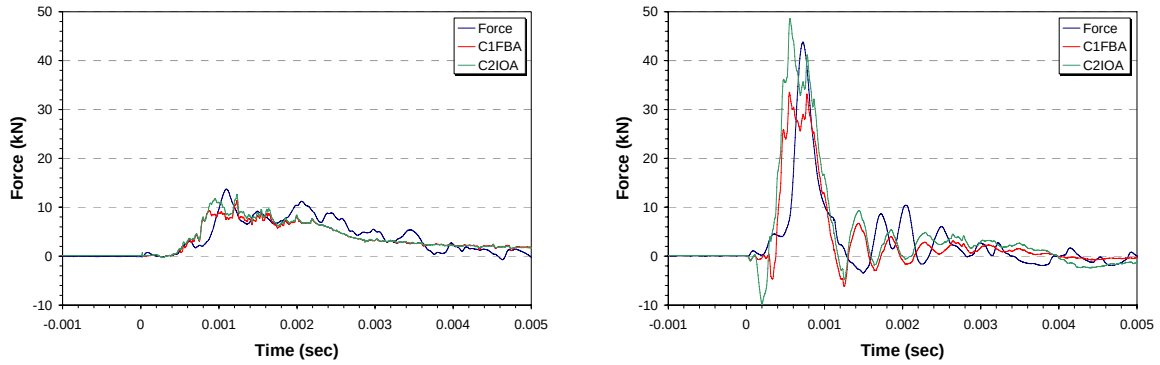


*Figure 15. Peak force and impulse delivered to the reference load cell as a function of standoff; the + sign after the label at 100 mm standoff indicates that the signal was clipped.*

The second set of observations from Figure 15 is concerned with the comparison of the three load signals for a given standoff distance. For the 200 mm standoff, it is seen that the three signals appeared to track each other well during the early stages of the explosion, but that the strain gauge signals then separated from the reference load cell signal. This behaviour differed from that observed during the drop tests, as was shown in Figure 9, when all three signals tracked each other throughout each test. The graphs also show that although the two strain gauge signals tracked each other relatively well, there were differences in signal amplitude during the peak load phase. These differences were even greater when the standoff distance was reduced to 50 mm, which corresponded to a significant increase in the explosive load.

Considering the steepest portion of the three signals on each plot, it can be seen that a large portion of the load cell signal lagged behind the strain signals by approximately 0.2 ms. It is surmised that this lag was due to the dynamics of the load transfer through the mounting arrangement that attached the FSLM specimens to the test rig, as shown in Figure 3. One can think of this arrangement as a series of four discrete masses (FSLM + steel mount adaptor + load cell + crossbeam). The explosive load applied to the bottom of the FSLM accelerated each one of these successive masses until the load cell tried to accelerate the crossbeam. However, because the crossbeam was more massive than the FSLM, adaptor and load cell, it 'pushed' back hard on the full assembly, which appeared temporarily to 'bounce back'. Only the reference load cell recorded this bounce because of its location within the system. Since the tibia was the lowest element, it did not record the bounce. At a lower load rate, this bounce did not occur.
In addition to the load history, the upper graphs of Annex E present the integral of the load recorded by the reference load cell. The integral of force over time is called the impulse. The left graph of Figure 16 presents the peak load and maximum impulse as a function of standoff distance. It is seen that the peak force increased monotonically as the standoff distance was reduced. Similarly, the maximum impulse increased as the standoff was first decreased from 200 mm down to 150 mm, and then to 125 mm. However, the maximum value of impulse was recorded for the 125 mm standoff. It decreased with decreasing standoff distance thereafter. This behaviour is attributed to

the change in failure mechanism at the distal end of the FSLM, which effectively interrupted the load path.

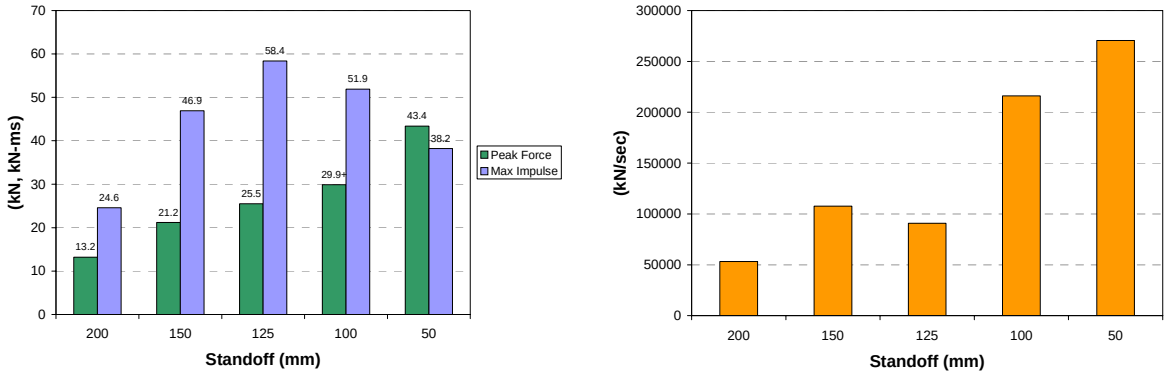


*Figure 16. (Left) Peak force and impulse delivered to the reference load cell as a function of standoff; the + sign after the label at 100 mm standoff indicates that the signal was clipped. (Right) Vertical load rate of the reference load cell measured from the signal rise.*

The right graph of Figure 16 presents the load rate as a function of standoff distance. These were computed from the average slope of the reference load immediately before it reached peak load. The load rate increased from 53,000 kN/sec up to 270,000 kN/sec as the standoff distance was decreased from 200 mm down to 50 mm. These load rates are 100 to 500 times greater than the typical load rate of 500 kN/sec that was recorded during the drop tests.

# 5. Conclusions

This work was successful in meeting the two objectives listed in section 1.3. For the first objective, the non-destructive drop test procedure made it possible to subject each FSLM model to multiple input loads so that the load cell built into the tibia could be calibrated and its accuracy verified. The 200 mm drops generated a peak force of approximately 4 kN at the reference load cell and a load rate of approximately 500 kN/sec. Under these input conditions, the FSLM's built-in load cell did exhibit a linear response. The slope of linear fits to the strain data was used to analyse the response of the built-in load cell. The following observations were made:

- The linearity for each individual drop test was very good, resulting in goodness-of-fit values ($R^2$) greater than 0.99 in all cases;
- The slope of the linear fits changed from one drop to the next, suggesting that a greater portion of the load was transmitted through the tibia after the first drop. It is surmised that this was due to a 'softening' of the glue joints_(polyamide), which changed the proportional load distribution between the tibia and fibula;

- The slope for the two compression channels were similar and consistent, but did exhibit up to 7% difference for the same leg;
- There were significant differences in the slope for different legs, up to 18%, which is surmised to be mostly due to slightly different load paths from leg to leg. While the manufacturing process[1] could account for the differing load paths there could be other reasons for the variations in slopes, such as:
    - Variations in the physical placement of strain gauges, which would produce differing signal levels;
    - Effects from boot fitment between legs,

For the second objective, the FSLM models were subjected to various explosive inputs. These tests generated peak loads that were up to 10 times greater than with the drop tests. The loading rate also increased significantly, ranging from 50,000 kN/sec to 270,000 kN/sec. The following observations resulted from the explosive tests:

- Varying the standoff is an effective technique to control the strength of the explosive input into the FSLM;
- The spring steel band in the sole of the boots was a good target for use with flash x-ray radiography in order to quantify the relative strength of the explosive input into the FSLM model. The velocity of the steel band was inversely proportional to the standoff, varying from 8 m/s up to 43 m/s as the standoff was decreased;
- The physical damage to the footwear varied from superficial abrasions and tears at 200 mm, to complete destruction of the hind foot at 50 mm. The sole of the boot was breached at 125 mm;
- The calcaneus and talus bones provided the most reliable and consistent response to explosive input. The calcaneus was intact at 200 mm and 150 mm, suffered a single fracture at 125 mm, and multiple fractures at 100 mm and 50 mm. The smallest standoff distance resulted in the greatest number of fragments;

[1] Since originally writing this report, the authors have learned of changes to the manufacturing process for the FSLM specimens. The polyamide glue used to bond critical load path components (e.g., calcaneus, talus, tibia and fibula) has been replaced with a form of synthetic gel. In addition, the leg bones are now positioned accurately in an alignment jig prior to bonding, the joint spaces are filled with measured volumes of synthetic gel, and a multi-layered heel pad has been added to the bottom of the leg assembly. With these improvements to the manufacturing process, the authors expect that variations in geometry from leg to leg is reduced, which would lead in a commensurate reduction in the slope from leg to leg, should a similar investigation to the work described in this report be carried out.

The main conclusion from this test program is that it is feasible to build in a 'disposable' load cell within the tibia bone of a modified FSL. The accuracy and repeatability of this built-in load cell will be less than for a high-precision metallic load cell due to the frangible nature of the FSLM, which makes it impossible to calibrate the built-in load cell over the full range of application. Nevertheless, the FSLM offers a practical alternative for tests with a high risk of damage to an anthropomorphic mannequin.

# 6. References


1. DM Bergeron, CG Coley, MS Rountree, IB Anderson and RM Harris, "*Assessment of Foot Protection Against Anti-Personnel Landmine Blast Using a Frangible Surrogate Leg*", Proceedings of the 2001 UXO conference, New Orleans, USA, April 2001.
2. DM Bergeron, RJ Swinton and MJ Footner, "*Performance of the AIGIS PPE 100 Footwear Against Anti-Personnel Landmine Blast*", DSTO Report TR-1613, Defence Science and Technology Organisation, Australia, 2004.
3. DM Bergeron (Editor), *Test Methodologies for Personal Protective Equipment Against Anti-Personnel Mine Blast*, RTO Technical Report TR-HFM-089, Research and Technology Organisation, NATO, 2004.
4. Private communication.
5. RM Harris, MS Rountree, RA Hayda, LV Griffin, SJ Mannion and T Bice, "*The Efficacy of Current Landmine Protective Footwear: Changes in Medical Outcomes*", Proceedings of the 2001 UXO conference, New Orleans, USA, April 2001.
6. PW Cooper, *Explosives Engineering*, Wiley-VCH, 1996.

# Appendix A: Strain Gauges Wiring and Connections

The following diagram shows the strain gauge placement, their connections and the bridge completion wiring.

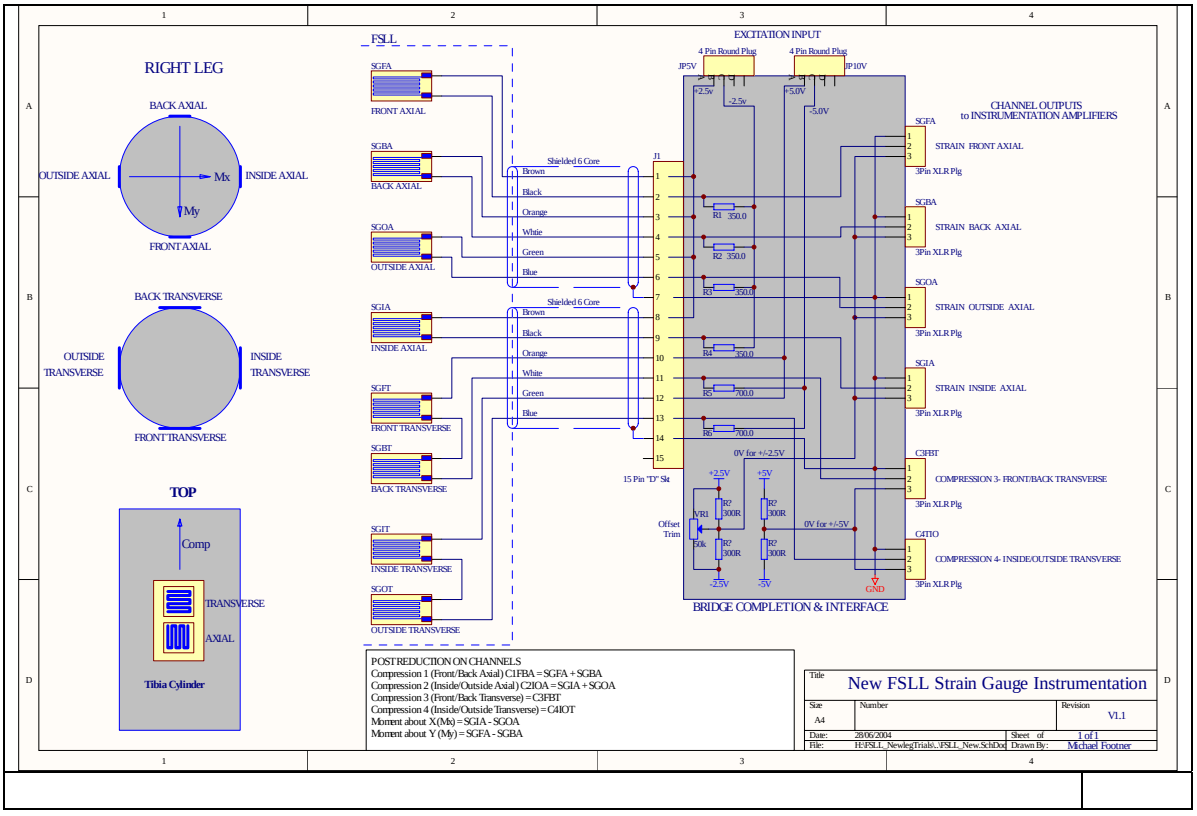

# Appendix B: Calibration of Bending Moments

The simple calibration of the bending moment was performed for each leg using a static load method. After positioning a leg in the appropriate direction, a load was applied transversely to the distal end of the leg by pulling a string that was attached around the boot. The other end of the string was tied to a spring scale in order to measure the static load, which varied from 0 to 4 kgf or 0 to 39.2 Newton. The moment arm between the location of the strain gauges and the string was approximately 0.4 m. Once the load was stabilised, strain gauge data was recorded for the individual strain gauges. An average strain value was then computed for each strain gauge, and these average values were finally subtracted in accordance with the criteria defined in Table 1 to compute the bending strain. The following table lists the values computed using this technique. These values are also plotted below.

*Average values of strain as a function of the applied $M_x$ moment for each leg.*

| Torque (Nm) | FSLM #1 (uS) | FSLM #2 (uS) | FSLM #3 (uS) | FSLM #4 (uS) | FSLM #5 (uS) | **Average (uS)** |
|---|---|---|---|---|---|---|
| 0.000 | 444.920 | 657.149 | 396.139 | -140.446 | 858.513 | **443.3** |
| 3.923 | 686.626 | 868.801 | 571.610 | 67.969 | 1038.261 | **646.7** |
| 7.846 | 912.727 | 1096.521 | 772.049 | 278.927 | 1263.207 | **864.7** |
| 11.768 | 1166.339 | 1329.557 | 973.182 | 490.926 | 1490.117 | **1090.0** |
| 15.691 | 1406.080 | 1562.710 | 1182.638 | 709.860 | 1715.640 | **1315.4** |

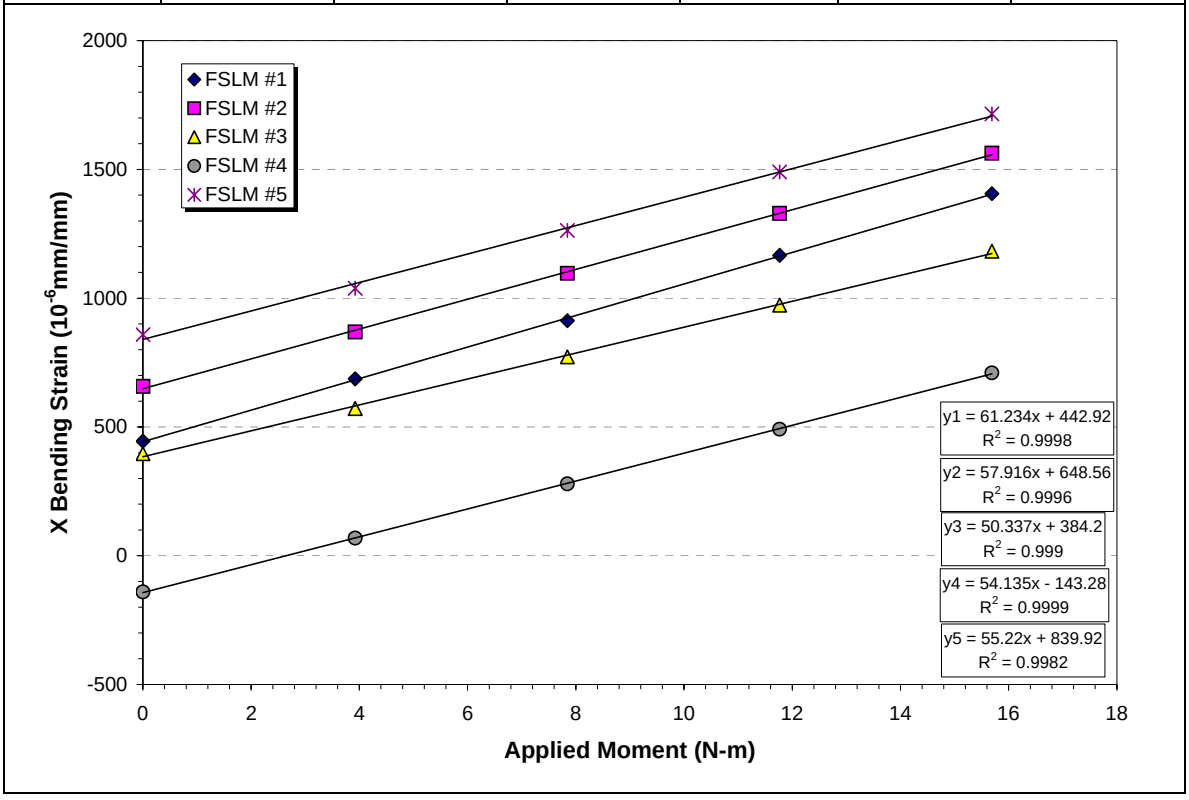

It is evident that by using individual strain gauges, the bending strain could not be zeroed for a zero bending load. As a result, the data exhibits large variations. It was therefore decided to apply a baseline correction to the data, as if the strain gauges had been wired in a bridge configuration and zeroed before a test. The following table and plot show the corrected data.

*Baseline corrected average values of strain as a function of the applied $M_x$ moment for each leg.*

| Torque (Nm) | FSLM #1 (uS) | FSLM #2 (uS) | FSLM #3 (uS) | FSLM #4 (uS) | FSLM #5 (uS) | **Average (uS)** |
|---|---|---|---|---|---|---|
| 0.000 | 0.000 | 0.000 | 0.000 | 0.000 | 0.000 | **0.000** |
| 3.923 | 241.706 | 211.652 | 175.471 | 208.415 | 179.748 | **203.398** |
| 7.846 | 467.807 | 439.371 | 375.910 | 419.373 | 404.693 | **421.431** |
| 11.768 | 721.419 | 672.408 | 577.043 | 631.372 | 631.603 | **646.769** |
| 15.691 | 961.161 | 905.560 | 786.499 | 850.306 | 857.126 | **872.130** |

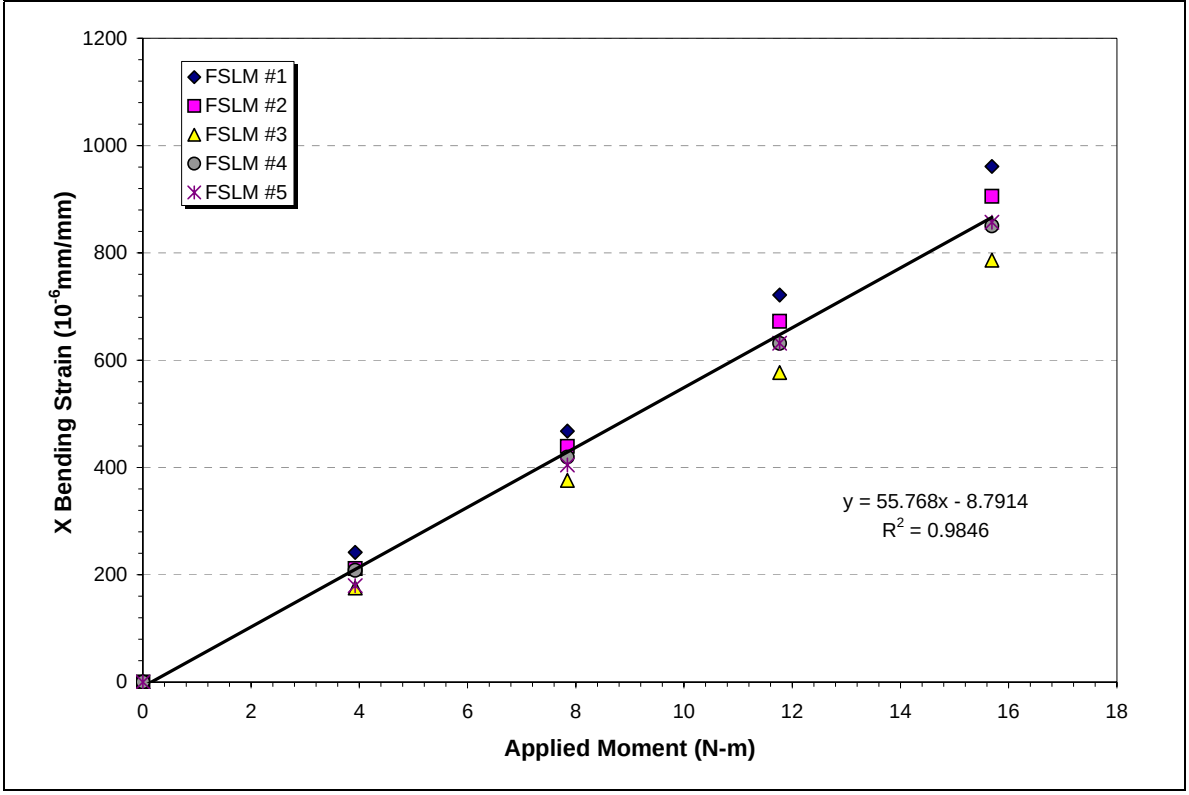


It is seen that this correction resulted in a considerable tightening of the data. The standard deviation for a given applied moment was between 7.5% and 13.2% from leg to leg. The slope and offset of the linear fit for each leg is listed in the table below. The average slope was 55.768 Nm/microstrain with an average offset of –8.791 Nm. The standard deviation for the slope was 7.3%. This variation is well within the accuracy of the calibration method used.

*Summary of $M_x$ slope, offset and goodness of fit data for the linear fits to each leg.*

| | FSLM#1 | FSLM#2 | FSLM#3 | FSLM#4 | FSLM#5 | Average |
|---|---|---|---|---|---|---|
| Slope | 61.234 | 57.916 | 50.337 | 54.135 | 55.220 | 55.768 |
| Offset | -2.000 | -8.588 | -11.939 | -2.831 | -18.598 | -8.791 |
| $R^2$ | 0.9998 | 0.9996 | 0.9990 | 0.9999 | 0.9982 | 0.9846 |

The same process was applied in the perpendicular direction to determine the bending response about the *y*-axis. The values obtained are listed and plotted in the table below.

*Average values of strain as a function of the applied $M_y$ moment for each leg.*

| Torque (Nm) | FSLM #1 (uS) | FSLM #2 (uS) | FSLM #3 (uS) | FSLM #4 (uS) | FSLM #5 (uS) | **Average (uS)** |
|---|---|---|---|---|---|---|
| 0.000 | 61.843 | -579.817 | -377.182 | 33.638 | -70.165 | **-186.3** |
| 3.923 | 546.411 | -97.445 | 39.880 | 473.934 | 367.010 | **266.0** |
| 7.846 | 1013.524 | 415.790 | 503.641 | 926.829 | 836.088 | **739.2** |
| 11.768 | 1482.372 | 895.850 | 945.093 | 1376.026 | 1280.777 | **1196.0** |
| 15.691 | 1969.252 | 1389.550 | 1400.069 | 1858.398 | 1754.942 | **1674.4** |

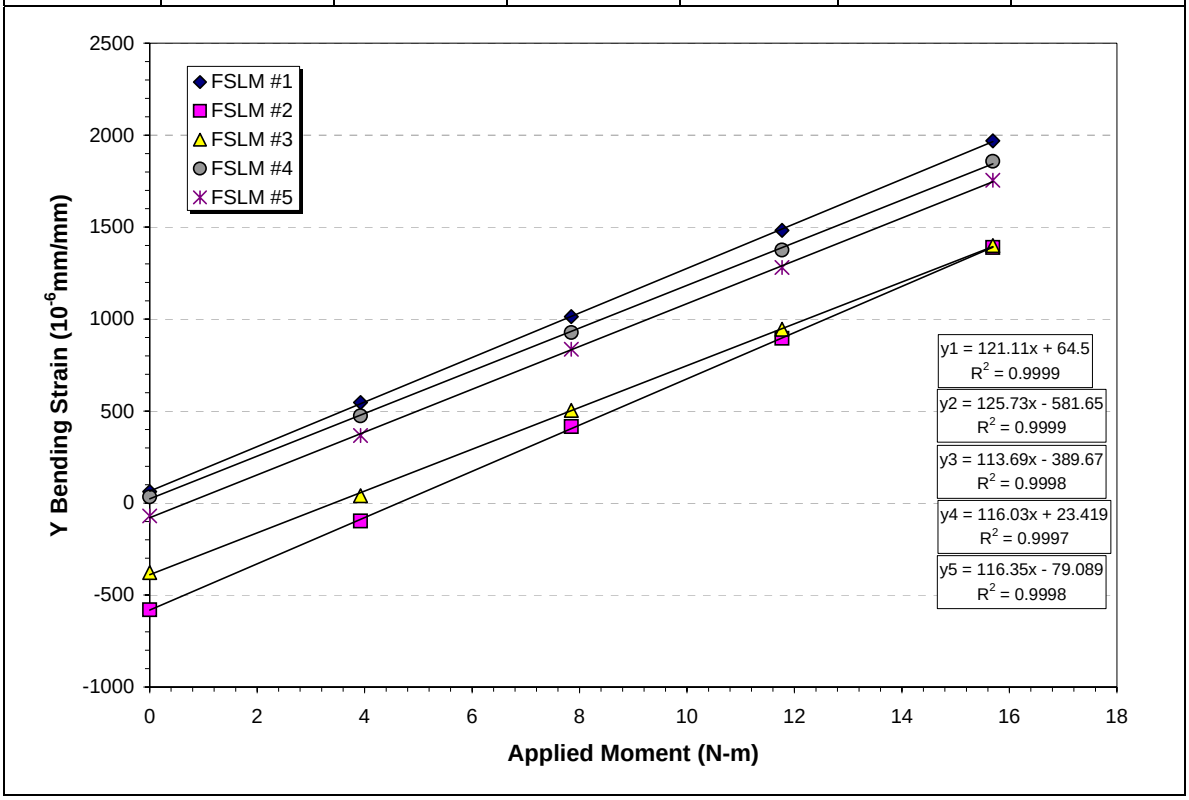


Again, the use of individual strain gauges led to wide variations in offset, but the slopes appear similar. Applying a baseline correction to the data, as if the strain gauges had been wired in a bridge configuration and zeroed before a test, produced the results listed and plotted in the following table.

*Baseline corrected average values of strain as a function of the applied $M_y$ moment for each leg.*

| Torque (Nm) | FSLM #1 (uS) | FSLM #2 (uS) | FSLM #3 (uS) | FSLM #4 (uS) | FSLM #5 (uS) | **Average (uS)** |
|---|---|---|---|---|---|---|
| 0.000 | 0.000 | 0.000 | 0.000 | 0.000 | 0.000 | **0.000** |
| 3.923 | 484.568 | 482.372 | 417.062 | 440.296 | 437.175 | **452.295** |
| 7.846 | 951.682 | 995.607 | 880.823 | 893.192 | 906.254 | **925.512** |
| 11.768 | 1420.529 | 1475.668 | 1322.275 | 1342.388 | 1350.942 | **1382.360** |
| 15.691 | 1907.410 | 1969.368 | 1777.251 | 1824.760 | 1825.107 | **1860.779** |

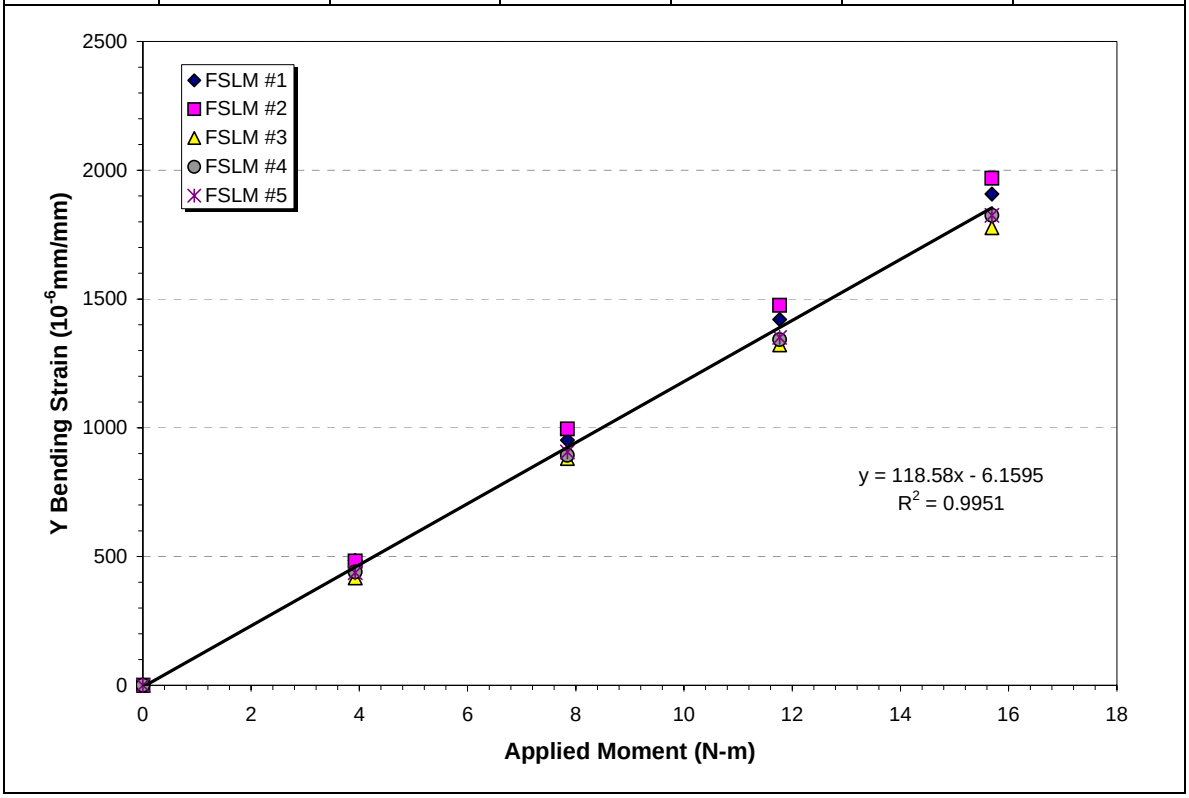


Once again, the correction tightened the data, resulting in a standard deviation between 4.1% and 6.6% from leg to leg for a given applied moment. The slope and offset of the linear fit for each leg is listed in the table below. The average slope was 118.58 Nm/microstrain with an average offset of –6.159 Nm. The standard deviation for the slope was 4.1%.

*Summary of $M_y$ slope, offset and goodness of fit data for the linear fits to each leg.*

| | FSLM#1 | FSLM#2 | FSLM#3 | FSLM#4 | FSLM#5 | Average |
|---|---|---|---|---|---|---|
| Slope | 121.11 | 125.73 | 113.69 | 116.03 | 116.35 | 118.58 |
| Offset | 2.657 | -1.829 | -12.484 | -10.218 | -8.924 | -6.159 |
| $R^2$ | 0.9999 | 0.9999 | 0.9998 | 0.9997 | 0.9998 | 0.9951 |

# Appendix C: Drop Test Results

The strain gauge compression was calibrated against the reference load cell using a series of drop tests. It was determined from preliminary tests (with leg #2) that the drops should be performed from a height of 200 mm. It was also noticed that the type of footwear fitted to the leg influenced the impact dynamics and the resulting peak force. This can be seen from the test results for leg #2 below, where the first four tests were performed with a new boot, while the last two tests were performed with an old boot. The sole of the old boot was worn out and its rubber was hardened, which increased the peak force significantly.

During each drop test, the data was recorded at a rate of 50,000 samples per second. During post-processing, data points were extracted at specific times from the reference load cell, and the four strain gauge channels. The times were selected from the time history of the reference load cell trace during the initial impact (the rebound phase was ignored) at 0.5 kN intervals. The strain gauge values were combined as per Table 1 to yield the two compression strains. The tables below list the results for the three tests performed with leg #1. The table also lists the average strain and the standard deviation for each force value. The maximum variation from test to test was of the order of 4%. A line was fitted through the data for each drop, and then through all the data for a given leg. The figures in this appendix show the results obtained for all legs.

*Value of axial compression strain extracted from three drop tests for channel C1FBA of leg 1.*

| F (N) | Test 1 | Test 2 | Test 3 | Average | Deviation | Percent |
|---|---|---|---|---|---|---|
| 500 | 284.8 | 275.3 | 296.6 | 285.6 | 10.6 | 3.7 |
| 1000 | 565.9 | 577.7 | 579.8 | 574.5 | 7.5 | 1.3 |
| 1500 | 857.3 | 890.2 | 888.0 | 878.5 | 18.4 | 2.1 |
| 2000 | 1156.7 | 1206.6 | 1237.8 | 1200.4 | 40.9 | 3.4 |
| 2500 | 1455.0 | 1519.0 | 1561.1 | 1511.7 | 53.4 | 3.5 |
| 3000 | 1742.7 | 1851.5 | 1884.5 | 1826.3 | 74.2 | 4.1 |
| 3500 | 2118.4 | 2190.0 | 2229.9 | 2179.4 | 56.5 | 2.6 |

*Value of axial compression strain extracted from three drop tests for channel C2IOA of leg 1.*

| F (N) | Test 1 | Test 2 | Test 3 | Average | Deviation | Percent |
|---|---|---|---|---|---|---|
| 500 | 282.1 | 270.3 | 293.1 | 281.8 | 11.4 | 4.0 |
| 1000 | 554.4 | 566.0 | 567.7 | 562.7 | 7.2 | 1.3 |
| 1500 | 844.8 | 876.9 | 872.8 | 864.9 | 17.5 | 2.0 |
| 2000 | 1140.5 | 1188.7 | 1215.1 | 1181.4 | 37.9 | 3.2 |
| 2500 | 1439.4 | 1498.7 | 1531.9 | 1490.0 | 46.8 | 3.1 |
| 3000 | 1725.7 | 1823.3 | 1850.0 | 1799.7 | 65.4 | 3.6 |
| 3500 | 2100.1 | 2160.4 | 2187.5 | 2149.3 | 44.7 | 2.1 |

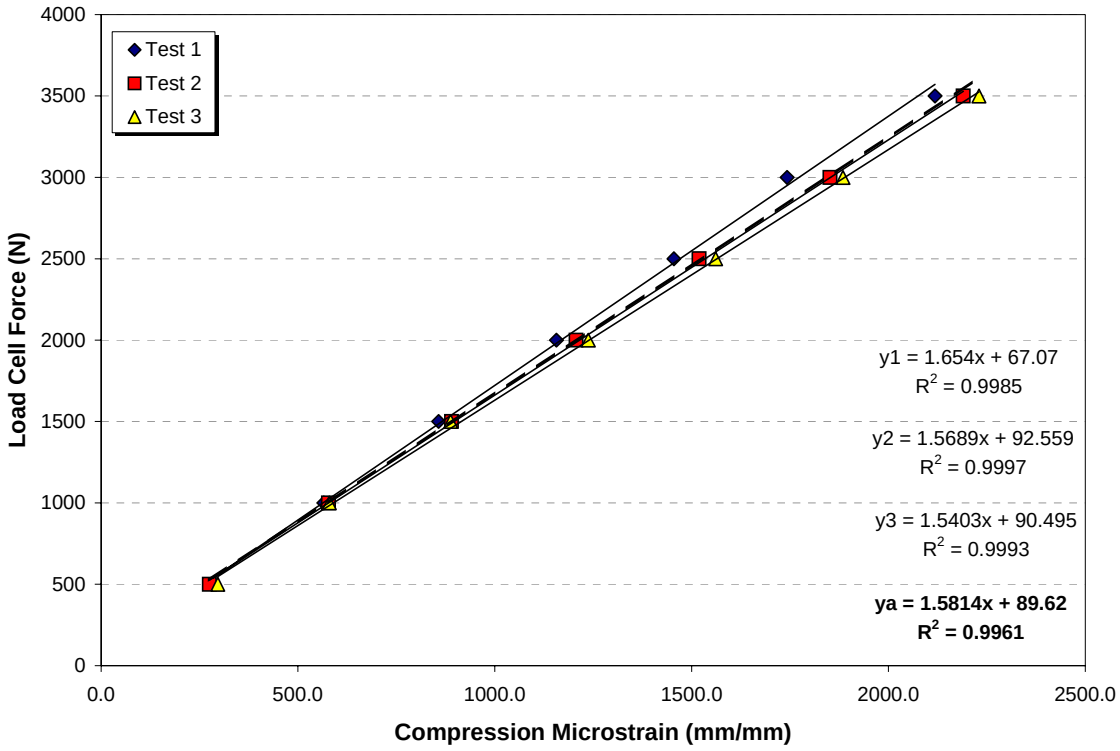


*Compression strain calibration derived from the Front and Back gauges, C1FBA, for leg 1.*

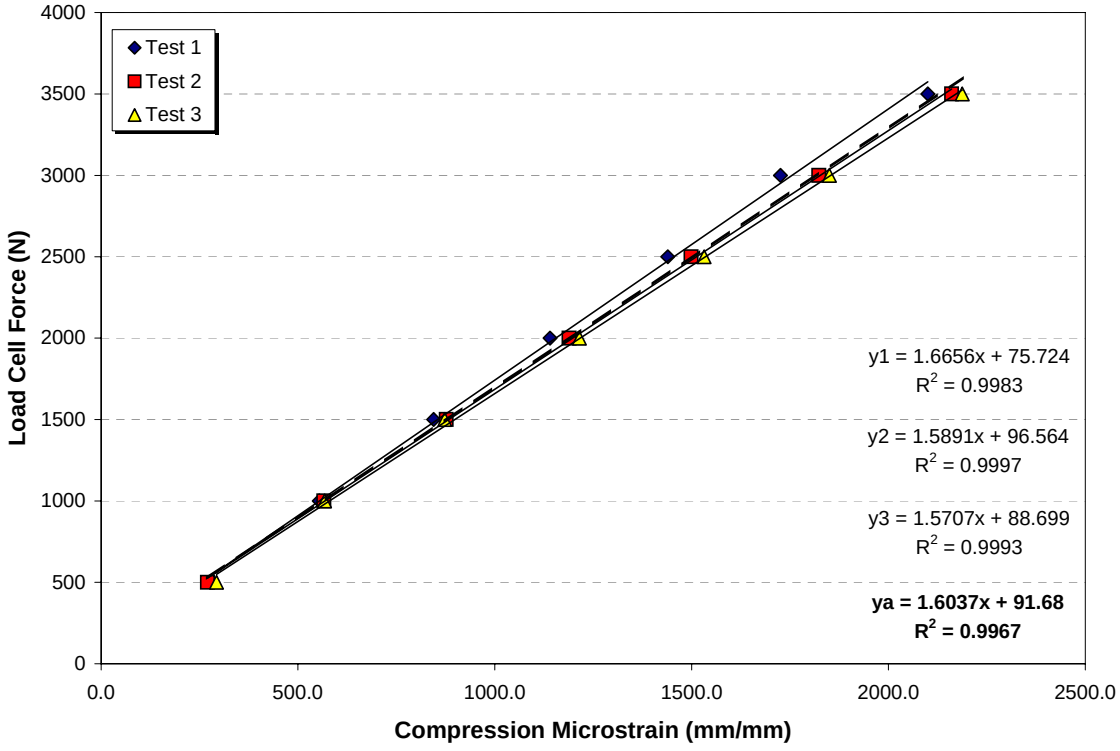


*Compression strain calibration derived from the Inside and Outside gauges, C2IOA, for leg 1.*

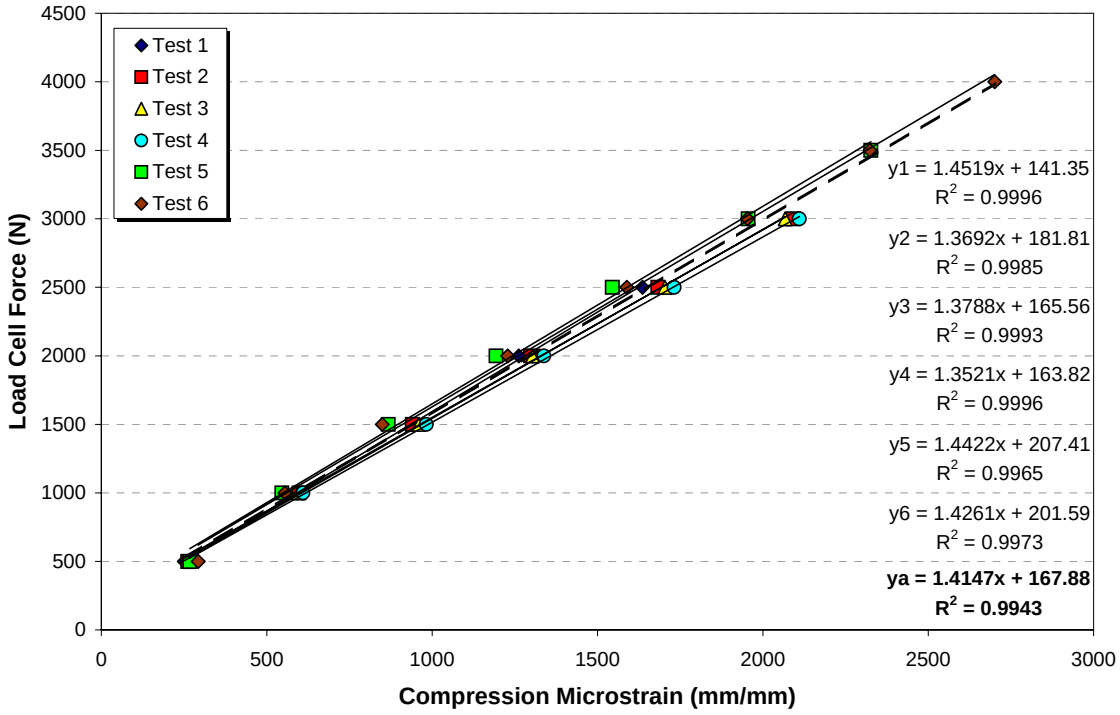


*Compression strain calibration derived from the Front and Back gauges, C1FBA, for leg 2.*

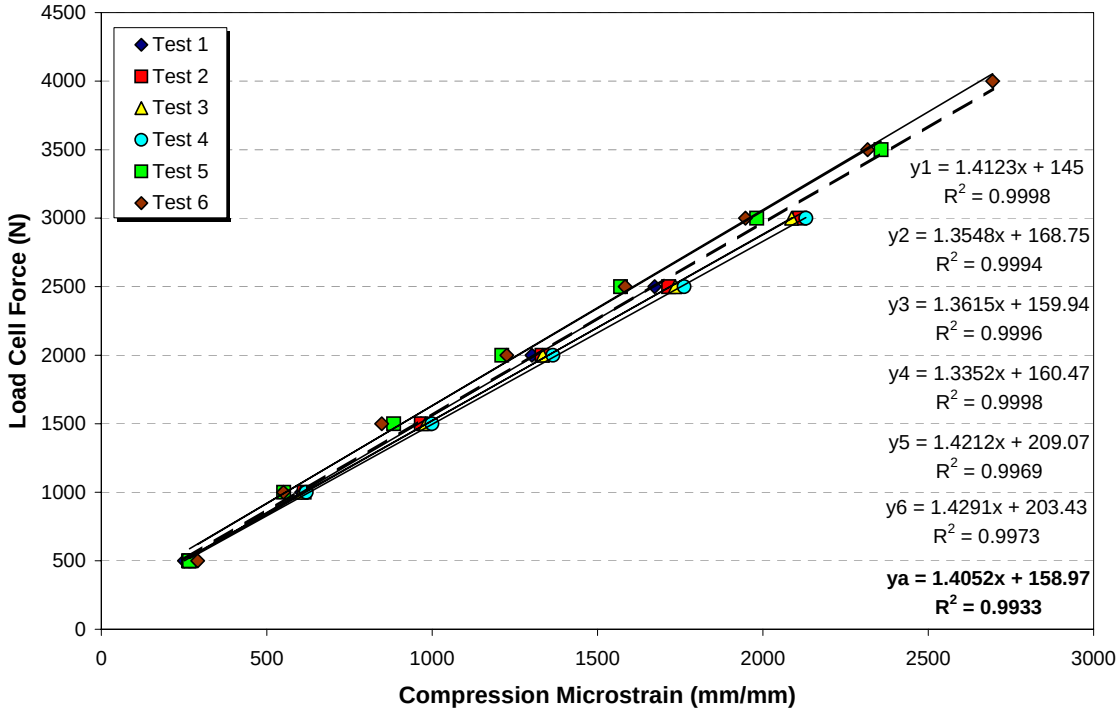


*Compression strain calibration derived from the Inside and Outside gauges, C2IOA, for leg 2.*

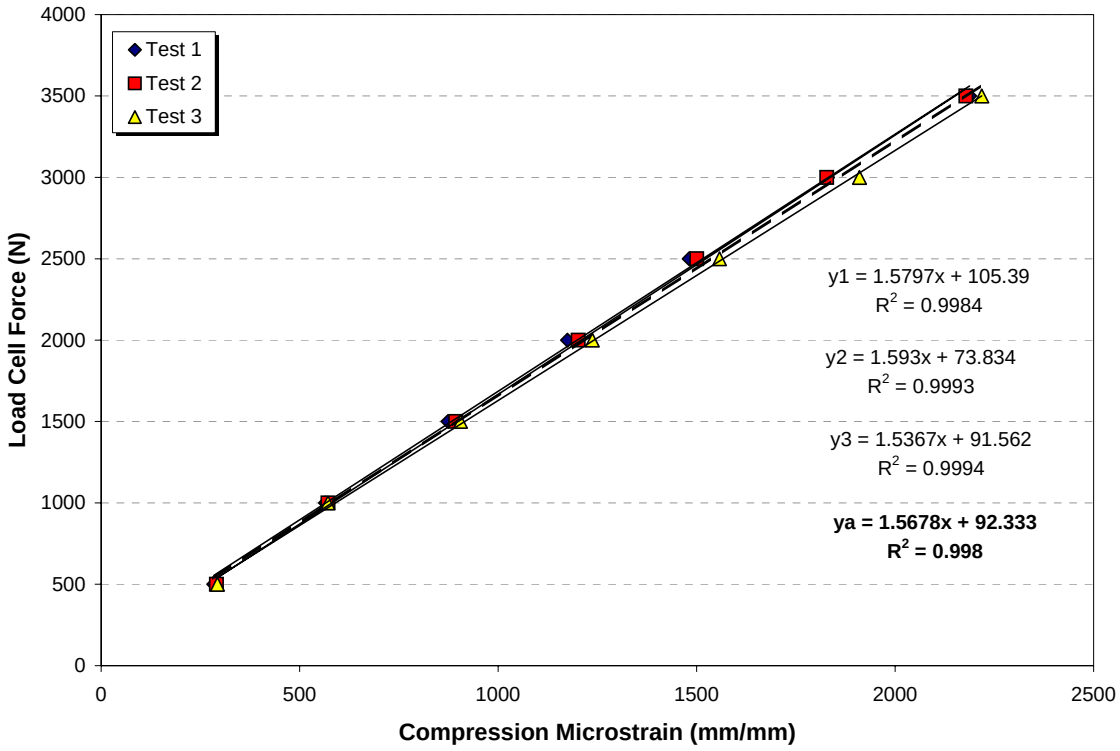


*Compression strain calibration derived from the Front and Back gauges, C1FBA, for leg 3.*

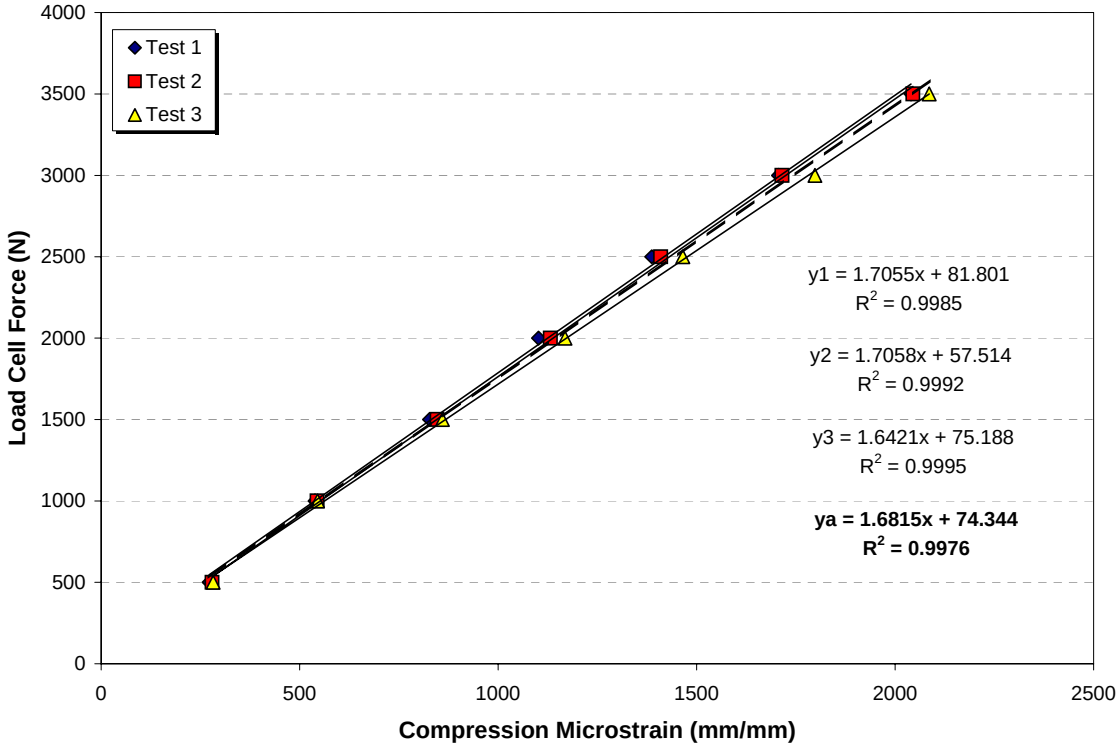


*Compression strain calibration derived from the Inside and Outside gauges, C2IOA, for leg 3.*

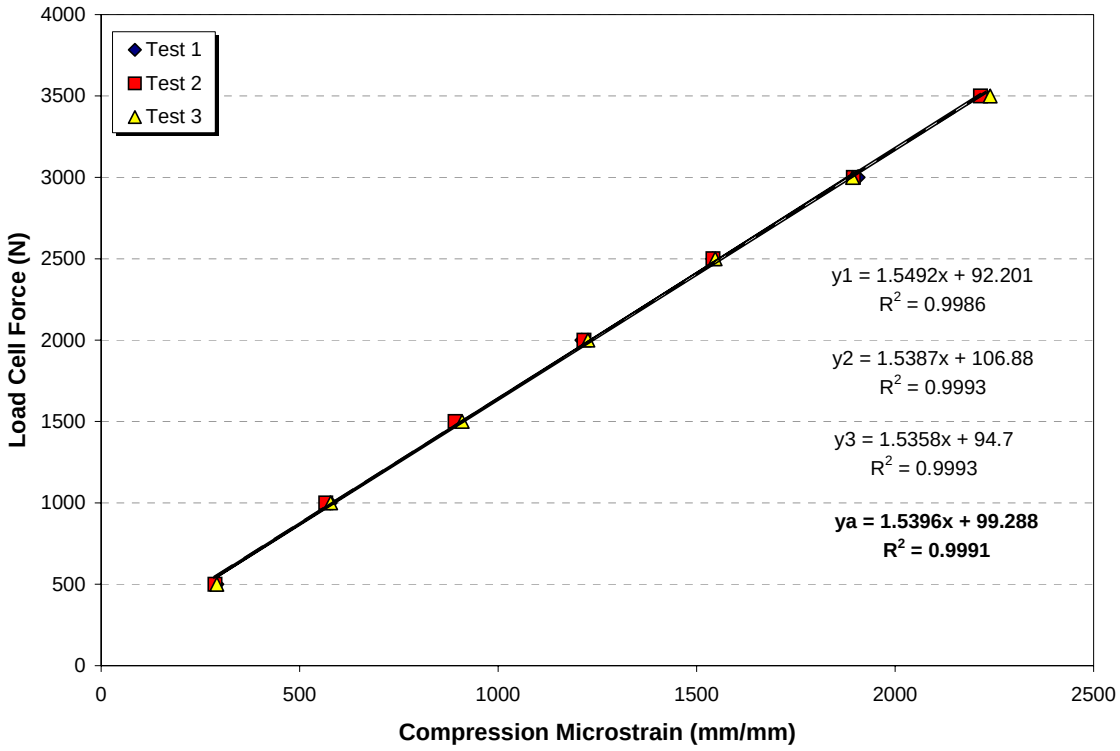


*Compression strain calibration derived from the Front and Back gauges, C1FBA, for leg 4.*

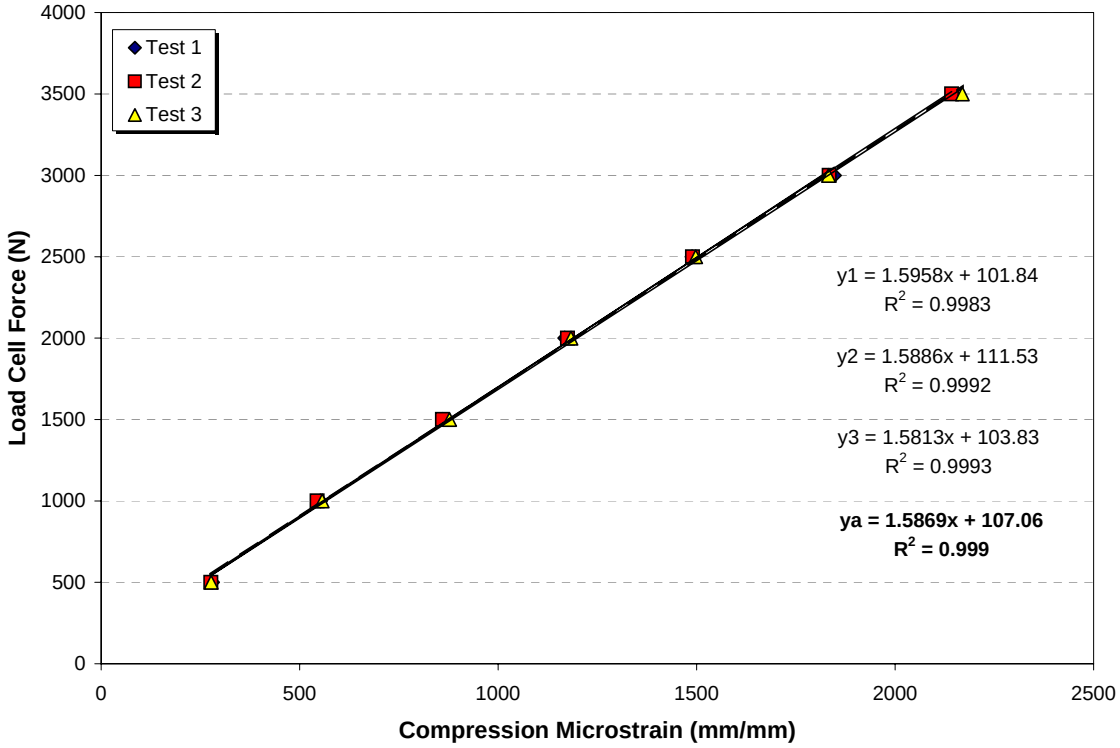


*Compression strain calibration derived from the Inside and Outside gauges, C2IOA, for leg 4.*

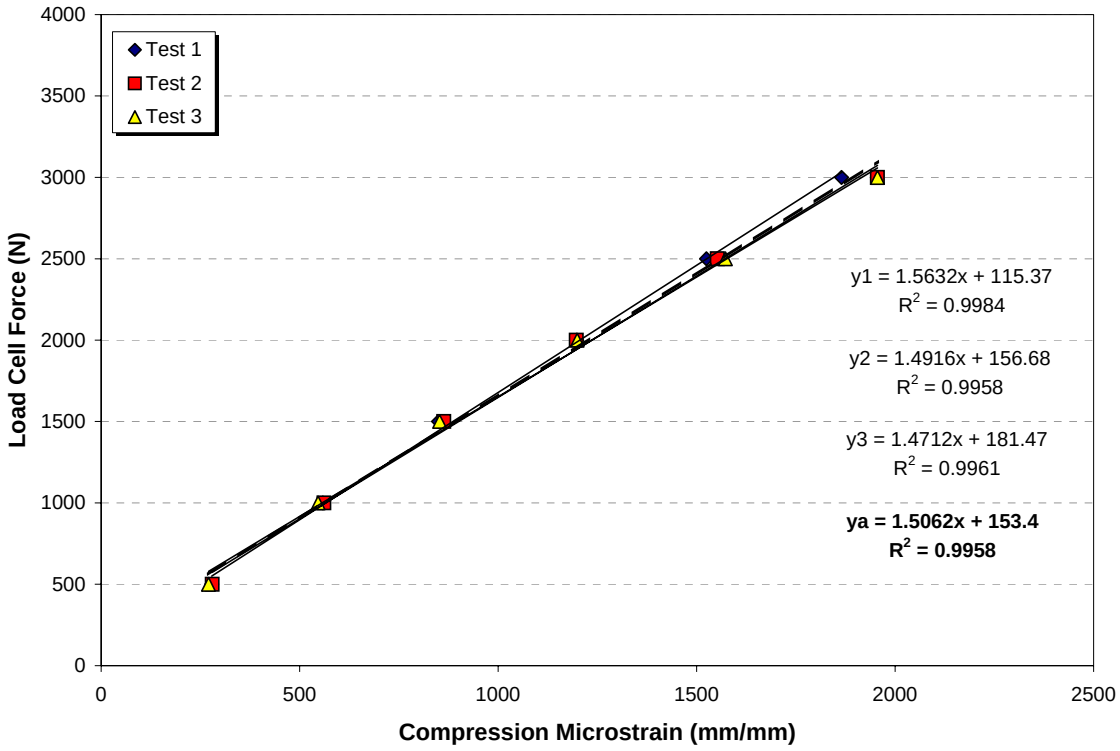


*Compression strain calibration derived from the Front and Back gauges, C1FBA, for leg 5.*

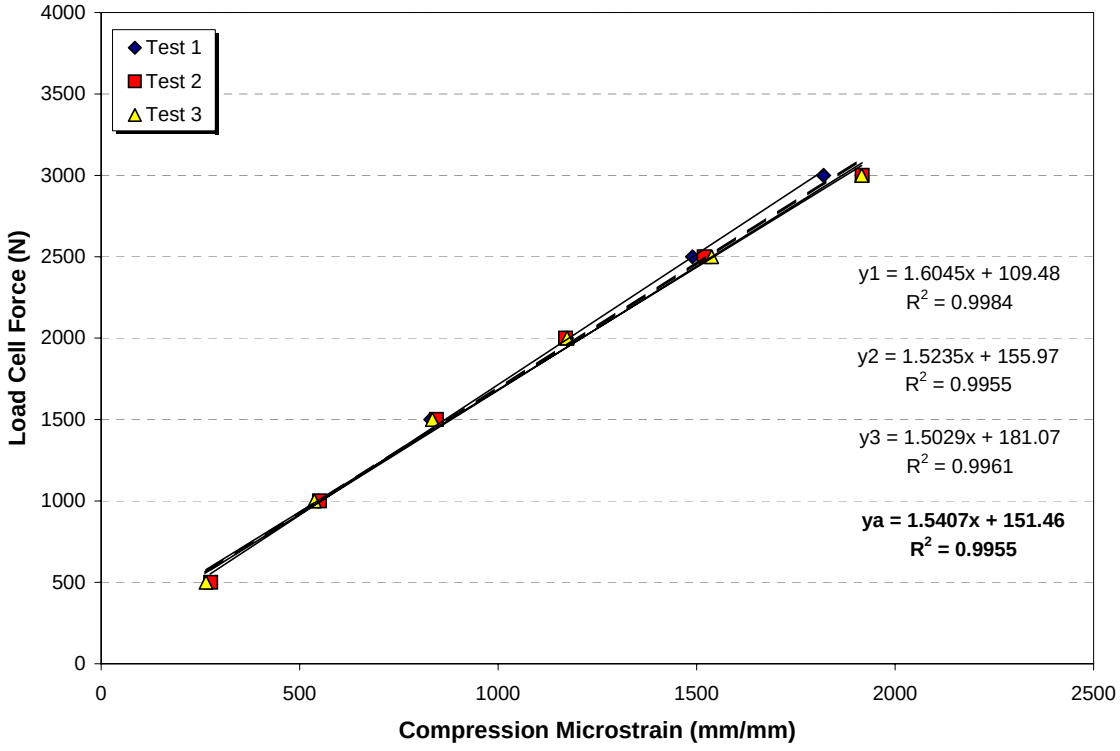


*Compression strain calibration derived from the Inside and Outside gauges, C2IOA, for leg 5.*

# Appendix D: Result Summaries for Explosive Tests

This Annex presents a detailed summary of the following post-test observations:

- State of the set-up upon entering the blast chamber immediately after the test
- Visual and physical inspection of the footwear
- Visual and physical inspection of the FSLM
- Inspection of the FSLM bones after removal of the gelatine

In addition, the authors present a summary of the results sought after changing the blast input conditions through standoff. Pictures supplement the information.

## Test 313-16: 200 mm Standoff

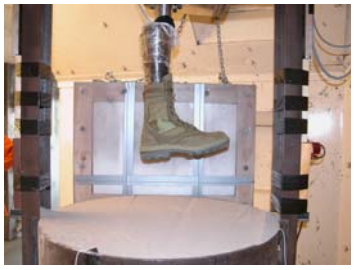
Picture A


Picture B


Picture C


Picture D


Picture E


Picture F

Picture A: Initial set-up showing the 200 mm standoff above the surface

Picture B: Only superficial damage to the boot could be observed

Picture C: Damaged gelatine around the ankle was easy to remove later

Picture D: Applying pressure revealed a dislocation to the ankle joint

Picture E: Applying pressure revealed a break across the top of the foot

Picture F: Broken bones of the mid-foot after partial removal of the gelatine

**Initial Observations**

The strength of the explosion caused a break of the head of the tibia across the pin insert and the whole leg was hanging by the instrumentation cable bundle. Internal damage to the foot was not apparent from the initial observations. Upon removal from the test rig, the leg had lost its pre-test rigidity, indicating that damage had occurred to the ankle and mid-foot.

**Damage to the Footwear**

The explosion imparted only minimal external damage to the boot. Soot and dust covered the outside of the boot, which was not breached otherwise. Sand abrasion was apparent on the outside of the boot, as shown in Picture B, and under the heel portion of the rubber sole. Upon closer inspection, minor cracks of the rubber sole were also found in the heel portion.

**Damage to the FSLM**

Removing the boot revealed that the explosion had driven the boot upward so hard

that the gelatine between the bottom of the calcaneus and the inside of the boot had been crushed (Picture C). The gelatine could be peeled by hand to expose the rear portion of the calcaneus. Applying pressure to the ankle showed that extensive dislocation of these bones had occurred. There was also extensive dislocation and multiple bone breaks in the mid-foot, as shown in Pictures E and F.

**Debridement and Inspection of the FSLM Bones**


The gelatine was stripped from the FSLM to expose multiple fractures to the metatarsal and tarsal bones, including a fracture forward of the talus. The calcaneus was not fractured and the talus had not been crushed. The fibula was intact while the tibia was broken at its proximal end, near the end of the metal pin insertion. This break does not correlate with the results from similar experiments with cadavers [5]. It is therefore considered to be an artefact of the mounting method used to attach the leg to the test fixture and would likely not occur in a real life accident.

**Overall Assessment of the Damage**

The 200 mm standoff distance was selected to minimise the damage to the FSLM. Particular attention was given to damage to the calcaneus and talus bones. Since these bones did not suffer major fractures, it was decided that 200 mm would be the maximum standoff for this test series. The level of damage that occurred to the mid-foot was more extensive than anticipated.

## Test 313-17: 100 mm Standoff


Picture A


Picture B


Picture C


Picture D


Picture E


Picture F

Picture A: The long bones and the boot were damaged during the test

Picture B: Damage to the sole of the boot exposed the spring steel insert

Picture C: The boot was breached and allowed ingress of contaminants

Picture D: The skin and soft tissues were breached to expose a shattered calcaneus

Picture E: Removal of the skin exposed further damage to the mid-foot

Picture F: Upper view of the damage to the mid-foot

**Initial Observations**

Damage to the upper portion of the long bones was apparent due to the rotation of the FSLM and the angle it hung at (Picture A). The boot was breached and the bones of the ankle were exposed to reveal extensive contamination from dust and soot.

**Damage to the Footwear**

The boot was destroyed in the hind to mid-foot region (Picture A) while the front of the boot suffered only superficial damage. The sole was torn, exposing the steel spring insert (Picture B). Soot and dust covered the external surface. After removing the boot from the FSLM, ingress of contaminants was also seen inside the lower rear portion of the boot (Picture C). The sole insert was torn.

**Damage to the FSLM**

This FSLM had been left wrapped in plastic (used to prevent desiccation of the gelatine). Removing the boot and sock (Picture D) revealed that the skin and soft tissues were avulsed, leaving an open contaminated wound. The calcaneus had a

comminuted fracture with several large fragments about a vertical shear plane. Damage to the talus was also seen. The bones of the mid-foot were fractured or dislocated (Pictures E and F). There was a transverse fracture of the tibia immediately above the level of the built-in load cell. Such damage was not reported in cadaver tests performed in the United States [5], hence it was determined that this damage was an artefact of the current model and that it was not likely to happen in an actual mine accident.

**Debridement and Inspection of the FSLM Bones**


Upon removal of the gelatine from the FSLM, the fibula was found to be intact. The tibia had a transverse fracture immediately above the level of the built-in load cell. There were no apparent fractures to the distal end of the tibia and fibula. The metatarsals and tarsals suffered multiple fractures and dislocations. There were multiple fractures of the calcaneus, which had been sheared about a vertical plane through the middle of the bone.

**Overall Assessment of the Damage**

Reducing the standoff distance from 200 down to 100 mm resulted in a very significant increase of the damage to the FSLM. The boot, skin and soft tissues (in the heel region) were breached and allowed ingress of the detonation products and dust to contaminate the wound. The avulsion of soft tissues combined with the extent of bone damage would result in a high probability of a below-knee amputation (BKA).

## Test 313-18: 50 mm Standoff


Picture A


Picture B


Picture C


Picture D


Picture E


Picture F

Picture A: The FSLM completely broke off the test rig and hung from the cables

Picture B: The ankle disintegrated leaving the front of the foot relatively undamaged

Picture C: The ankle damage was apparent once the skin had been removed

Picture D: The front of the foot remained attached only by the simulated tendons

Picture E: Further dissection of the leg showed a mid-leg transverse fracture

Picture F: Several bone fragments were recovered from the blast chamber floor

**Initial Observations**

Picture A shows how the FSLM broke off near the upper extremity of the model and was left hanging by the instrumentation cables. The upper portion of the bone remained attached to the test rig. There was extensive damage to the boot and to the distal end of the FSLM. Boot, bone, and gelatine fragments were dispersed throughout the test chamber.

**Damage to the Footwear**

The boot was destroyed in the hind to mid-foot region (Pictures B and C) while the front of the boot suffered less damage. Tears ran forward into the rubber sole and minor fractures were present in the external front portion of the rubber sole. The disintegration of the sole left the rear half of the spring steel insert fully exposed. Soot and dust covered the external surface and major portions of the inside. The lower part of the boot-upper was destroyed in the heel region.

**Damage to the FSLM**

There was a traumatic amputation of the forward portion of the foot as a result of the complete disintegration of the ankle. Breaching of the boot, skin, and soft tissues exposed the distal end of the model to contamination from the detonation products and dust (Picture C). The front portion of the foot remained complete as a whole piece and stayed attached to the leg by two simulated tendons (Picture D). There were transverse fractures of the tibia and fibula bones.

**Debridement and Inspection of the FSLM Bones**


Debridement of the gelatine from the FSLM clearly showed a mid-fibula fracture and a 1/3rd distal fracture of the tibia. The tibia also fractured at the proximal end through the metal pin attachment, an artefact of the mounting technique. All foot bones, with exception of the phalanges, suffered extensive comminution. These bones were avulsed during the traumatic amputation process. Soot and dust coated the bone fragments that had been recovered from the blast chamber as well as the distal end of the long bones. The calcaneus and talus were shattered into numerous small pieces.

**Overall Assessment of the Damage**

Further reducing the standoff distance from 100 mm down to 50 mm resulted in a substantial increase of the damage to the distal end of the FSLM. The boot, skin and soft tissues (in the heel region) were breached with avulsion of the ankle and mid-foot bones. The result was a typical traumatic amputation as noted in References [1] and [5]. The size of the calcaneus and talus fragments that were recovered was smaller than for the 100 mm test, showing that an increase of the blast input into the model resulted in more severe damage.

## Test 313-19: 150 mm Standoff

Picture A

Picture B

Picture C

Picture D

Picture E

Picture F

| | |
|---|---|
| Picture A: | Damage to the exterior of the boot consisted of abrasion and minor tears |
| Picture B: | The force of the explosion caused a tear to the inside sole of the boot |
| Picture C: | The boot displacement caused fissuring of the gelatine and penetration of the calcaneus through the bottom of foot |
| Picture D: | The fissuring extended right around to the upper surface of the foot |
| Picture E: | Removal of the gelatine exposed the broken bones of the mid-foot |
| Picture F: | The calcaneus and talus bones were dislocated from the tibia and fibula |

**Initial Observations**

The explosion had caused a break at the upper portion of the tibia and the FSLM was hanging from the test fixture. The boot was not breached, thus indicating that any injury would be contained.

**Damage to the Footwear**

The structural integrity of the boot was maintained (Picture A) but abrasion and minor tears of the outer surface of the boot were visible. The sole showed minor tears of the rubber on its lower surface. The explosion pushed the boot with sufficient force to cause an imprint of the calcaneus and a minor tear of the inside sole (Picture B). There was no penetration of contaminants in the boot.

**Damage to the FSLM**

Despite minimal damage to the boot, fissuring of the gelatine extended from the bottom of the heel right around the ankle (Pictures C and D). This indicated that there

had been significant vertical displacement of the forward portion of the foot relative to the ankle and long bones. Removal of the gelatine revealed extensive dislocation and fractures to the bones of the mid-foot. (Picture E). The tibia was fractured at its proximal end immediately below the end of the steel pin insert. Such damage was an artefact of the current model and was not likely to happen in an actual mine accident.

**Debridement and Inspection of the FSLM Bones**


Upon debridement of the gelatine from the FSLM, the fibula was found to be intact. The tibia had a transverse fracture above the level of the built-in load cell. There were no apparent fractures to the distal end of the tibia and fibula although there was a dislocation of the talus from the long bones. The metatarsals and tarsals suffered limited fractures and dislocations. There were no fractures of the calcaneus and talus. The bone group of the mid-foot (sub-talar group) suffered multiple dislocations.

**Overall Assessment of the Damage**

The intent of this test was to produce less bone damage than at 100 mm standoff, but more damage than at 200 mm. This was achieved since the level of damage to the mid-foot and to the ankle was similar to the 200 mm standoff case, except that there was complete dislocation of the talus from the tibia and fibula.

## Test 313-20: 125 mm Standoff


Picture A


Picture B


Picture C


Picture D

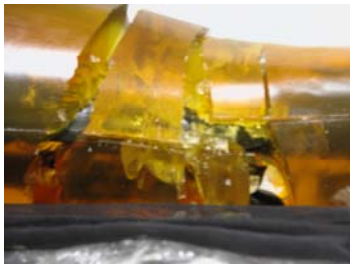
Picture E


Picture F

| | |
|---|---|
| Picture A: | The FSLM remained attached to the test rig but the long bones had broken |
| Picture B: | The sole of the boot was breached and pushed into the foot |
| Picture C: | The skin was breached under the heel and the plastic wrap was pushed in |
| Picture D: | There was a vertical break of the calcaneus near its mid-section |
| Picture E: | The mid-tibia break resulted in extensive fissuring of the gelatine |
| Picture F: | The front of the foot remained in one piece and the talus stayed attached to the tibia |

**Initial Observations**

This was the first and only test where the FSLM remained attached to the test fixture. There was, however, a transverse break of the fibula and tibia, which was apparent from the angle of the boot, relative to the top of the leg (Picture A). The sole of the boot had been breached (Picture B), but there were very few (none significant) separate boot fragments.

**Damage to the Footwear**

The sole of the boot was breached and pushed into the bottom of the foot (Picture B). Considering that the standoff had been decreased by only 25 mm relative to test 313-19, this was a significant change. Soot and dust covered the external surface. There was limited ingress of contamination into the rear portion of the boot and into the gelatine near the back of the foot (Picture C).

**Damage to the FSLM**

This FSLM had been left wrapped in plastic. After removing the boot and sock (Picture C), it was seen that a small amount of gelatine had been avulsed, resulting in an open contaminated wound. The calcaneus had a minimally displaced vertical fracture (Picture D). The talus was intact and remained attached to the tibia. The bones of the mid-foot were fractured or dislocated.

There were mid-shaft transverse fractures of the tibia and fibula.

**Debridement and Inspection of the FSLM Bones**


Debridement of the gelatine from the FSLM revealed multiple fractures to the metatarsals, tarsals, and to the proximal phalanges. There was single vertical fracture across the calcaneus in its mid-plane. The talus was intact and remained attached to the tibia. The tibia had a mid-shaft fracture. The fibula suffered a combination of mid-shaft and 1/3$^{rd}$ distal fractures, one being with a classic fragment.

**Overall Assessment of the Damage**

The small reduction of the standoff distance from 150 mm down to 125 mm produced the increased damage level as sought. This demonstrated the important effect that small changes in standoff distance have on the damage potential of a landmine. More importantly, it demonstrated the ability of the FSLM to change its response to relatively small changes in the blast input conditions.

# Appendix E: Load and Displacement Data

Each page of this Annex presents two graphs. The upper graph presents the vertical force history measured by the reference load cell and the two force histories recorded from the FSLM strain gauges. These three curves are superimposed on the same scale. The integral of the force measured by the reference load cell was computed and it is plotted on a separate scale. The lower graph presents the bending moments Mx and My measured by the FSLM's integral load cell. The moments were computed using the static calibration factors.

The reader should note that the scales on each graph have been held constant for ease of comparison.

# Test 313-16: 200 mm Standoff

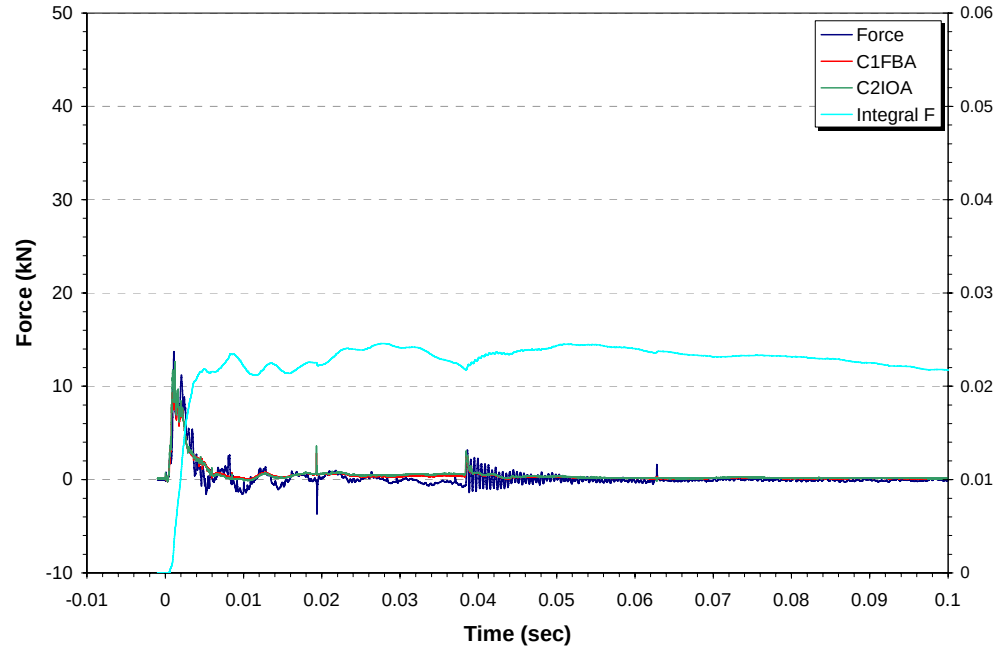


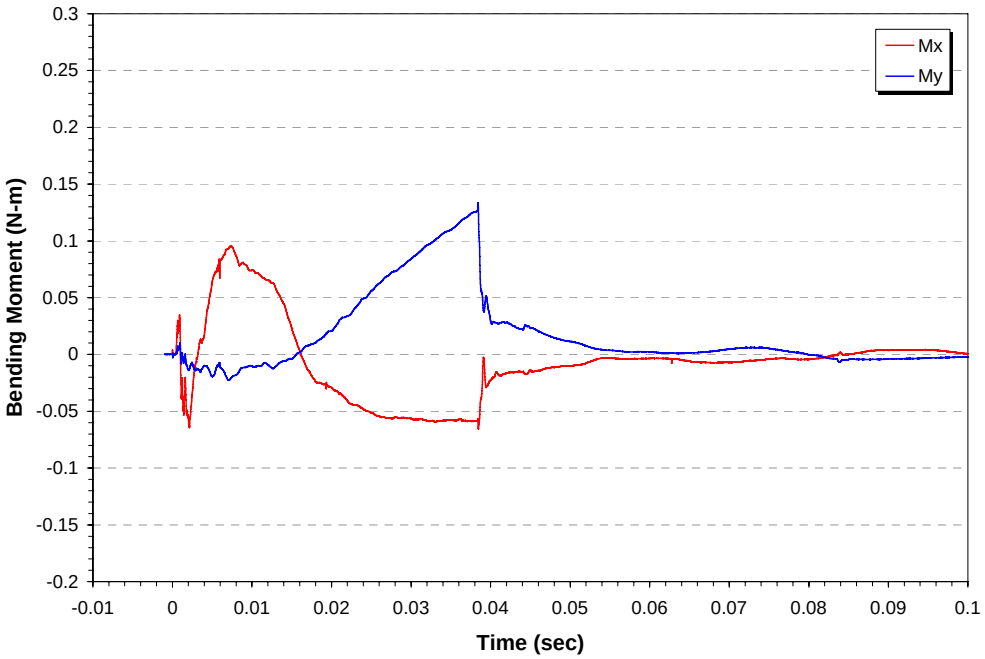

# Test 313-17: 100 mm Standoff

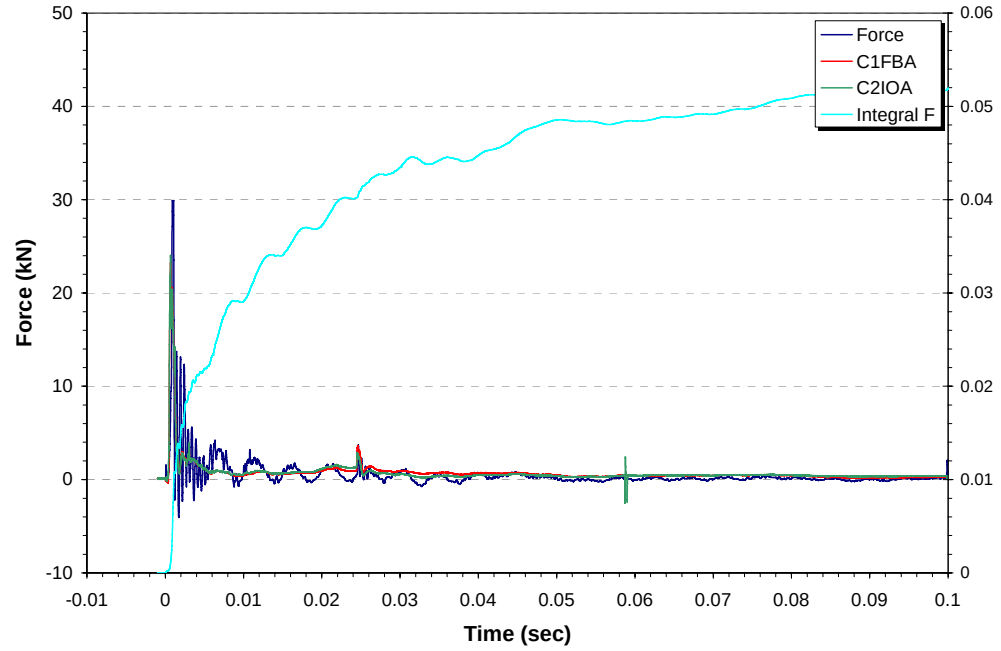


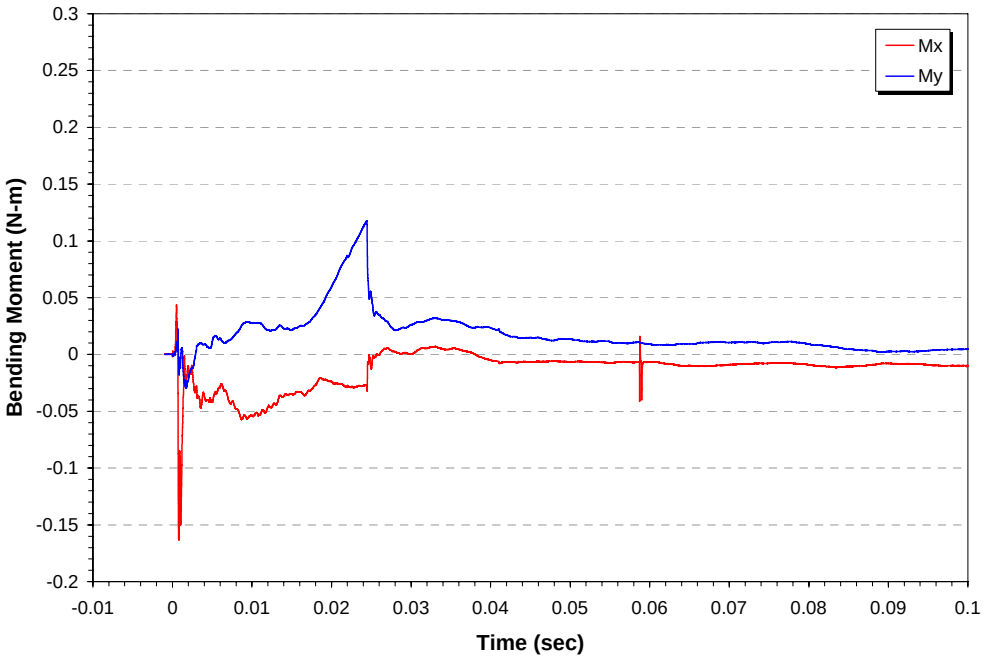

# Test 313-18: 50 mm Standoff

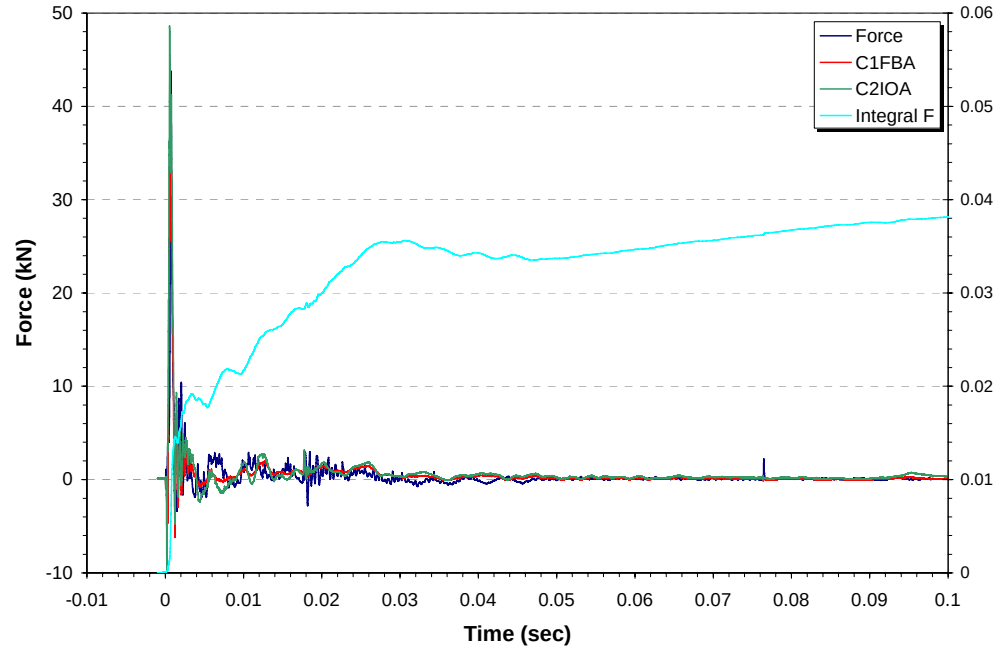


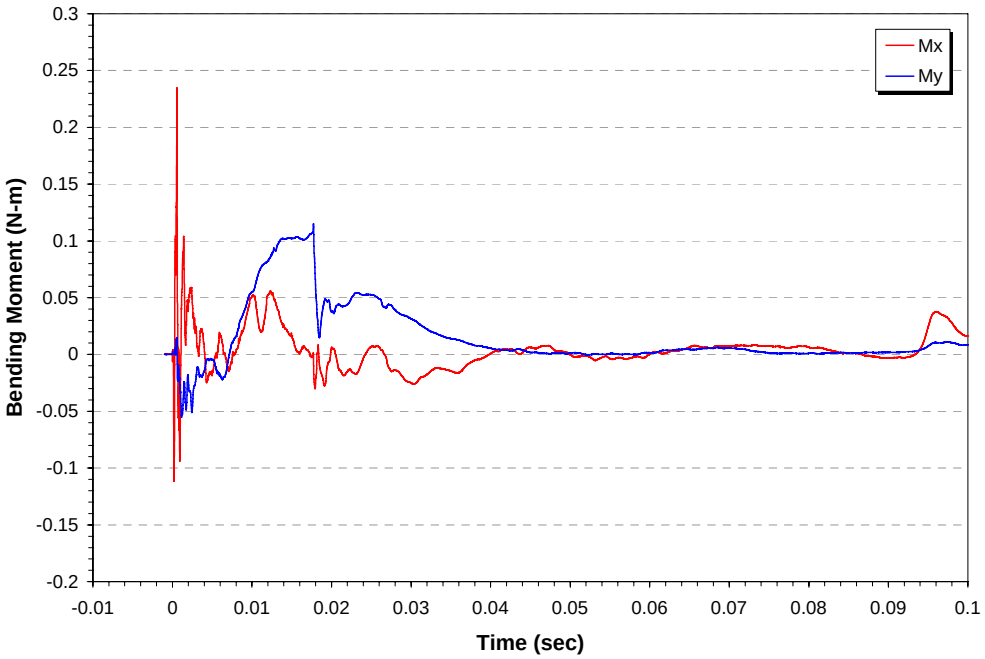

# Test 313-19: 150 mm Standoff

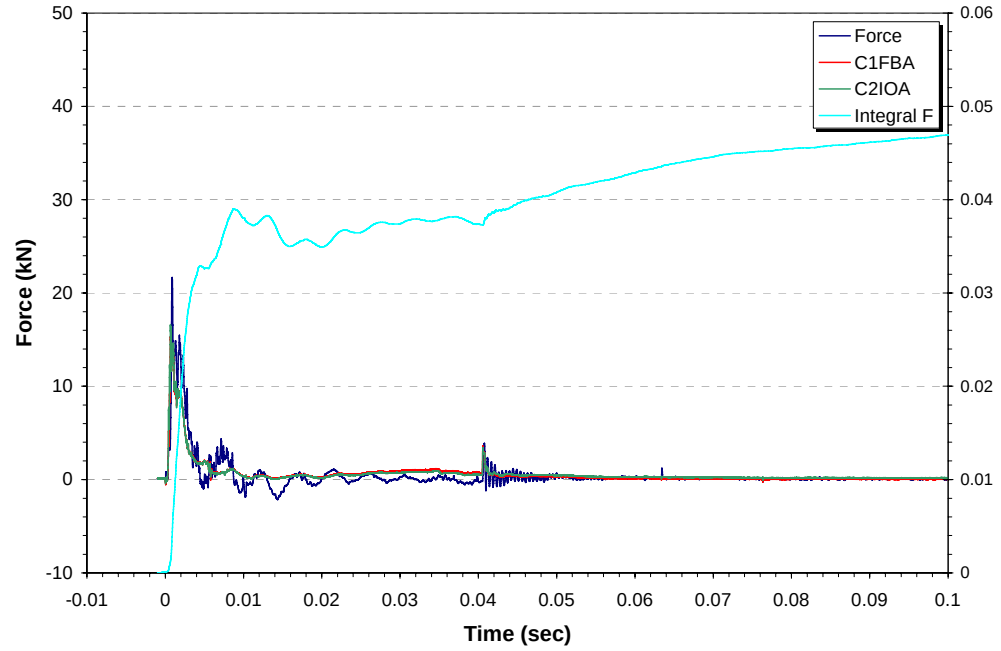


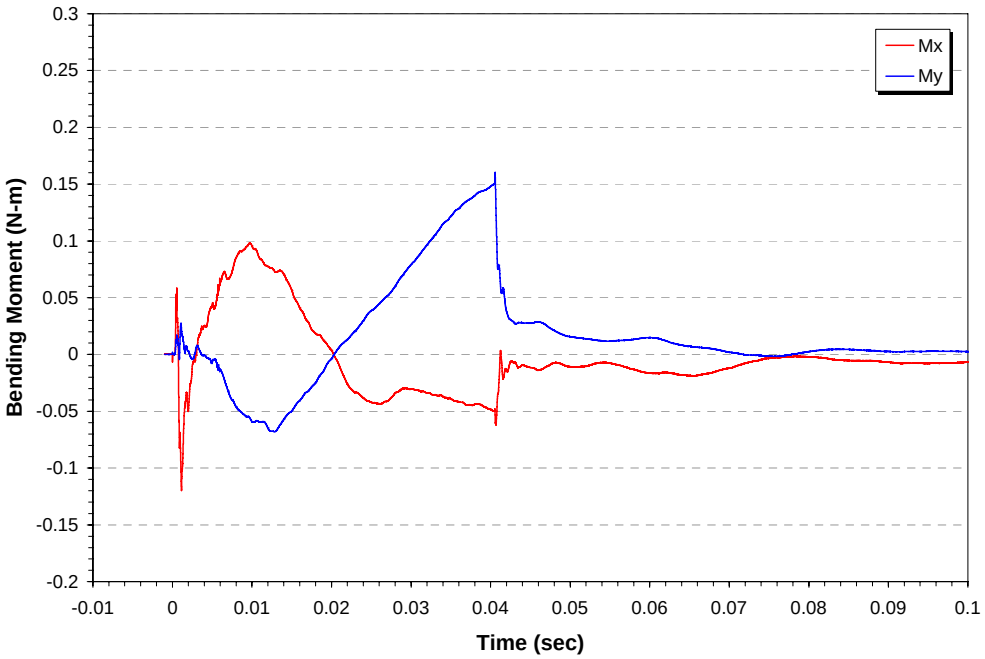

# Test 313-20: 125 mm Standoff

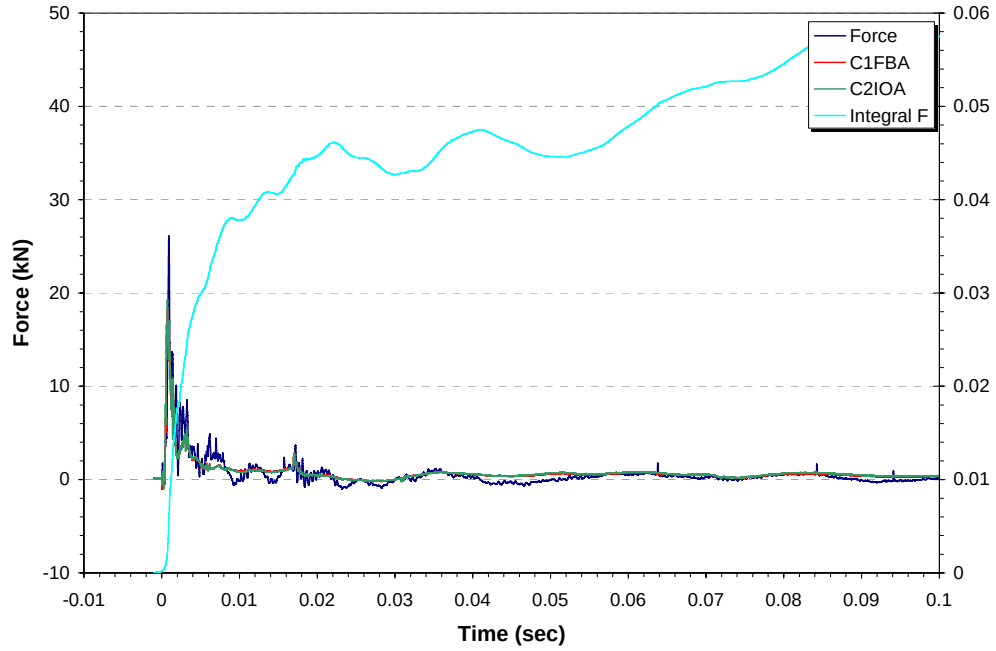


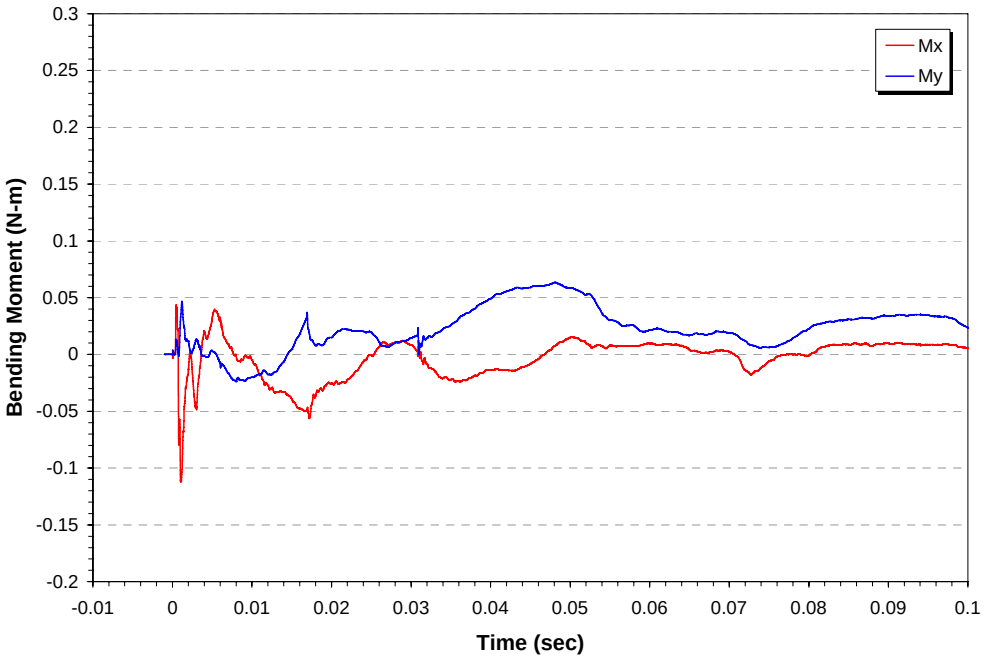

DISTRIBUTION LIST

Development and Calibration of a Frangible Leg Instrumented for Compression and Bending

M.J. Footner, D.M. Bergeron and R.J. Swinton

**AUSTRALIA**

| **DEFENCE ORGANISATION** | **No. of copies** |
|---|---|
| ***Task Sponsor*** | |
| DGLD | 1 Printed |
| **S&T Program** | |
| Chief Defence Scientist | 1 |
| Deputy Chief Defence Scientist Policy | 1 |
| AS Science Corporate Management | 1 |
| Director General Science Policy Development | 1 |
| Counsellor Defence Science, London | Doc Data Sheet |
| Counsellor Defence Science, Washington | Doc Data Sheet |
| Scientific Adviser to MRDC, Thailand | Doc Data Sheet |
| Scientific Adviser Joint | 1 |
| Navy Scientific Adviser | Doc Data Sht & Dist List |
| Scientific Adviser – Army | 1 |
| Air Force Scientific Adviser | Doc Data Sht & Dist List |
| Scientific Adviser to the DMO | 1 |
| **Systems Sciences Laboratory** | |
| Chief of Weapons Systems Division | Doc Data Sht & Dist List |
| Research Leader Land Weapon Systems | Doc Data Sht & Dist List |
| Head | 1 Printed |
| Task Manager (Roy Bird) | 1 Printed |
| Christopher Anderson | 1 Printed |
| *Author(s):* | |
| Michael Footner | 1 Printed |
| Denis Bergeron (C/o M. Footner) | 1 Printed |
| Robert Swinton | 1 Printed |
| **DSTO Library and Archives** | |
| Library Fishermans Bend | Doc Data Sheet |
| Library Edinburgh | 2 printed |
| Defence Archives | 1 printed |
| Library, Sydney | Doc Data Sheet |
| Library, Stirling | Doc Data Sheet |

| | |
|---|---|
| Library Canberra | Doc Data Sheet |
| **Capability Development Group** | |
| Director General Maritime Development | Doc Data Sheet |
| Director General Land Development | 1 |
| Director General Capability and Plans | Doc Data Sheet |
| Assistant Secretary Investment Analysis | Doc Data Sheet |
| Director Capability Plans and Programming | Doc Data Sheet |
| **Chief Information Officer Group** | |
| Director General Australian Defence Simulation Office | Doc Data Sheet |
| AS Information Strategy and Futures | Doc Data Sheet |
| Director General Information Services | Doc Data Sheet |
| **Strategy Group** | |
| Director General Military Strategy | Doc Data Sheet |
| Assistant Secretary Governance and Counter-Proliferation | Doc Data Sheet |
| **Navy** | |
| Maritime Operational Analysis Centre, Building 89/90 Garden Island Sydney NSW<br>Deputy Director (Operations)<br>Deputy Director (Analysis) | Doc Data Sht & Dist List |
| Director General Navy Capability, Performance and Plans, Navy Headquarters | Doc Data Sheet |
| Director General Navy Strategic Policy and Futures, Navy Headquarters | Doc Data Sheet |
| **Air Force** | |
| SO (Science) - Headquarters Air Combat Group, RAAF Base, Williamtown NSW 2314 | Doc Data Sht & Exec Summ |
| **Army** | |
| **ABCA National Standardisation Officer**<br>Land Warfare Development Sector, Puckapunyal | e-mailed Doc Data Sheet |
| SO (Science) - Land Headquarters (LHQ), Victoria Barracks NSW | Doc Data & Exec Summary |
| SO (Science), Deployable Joint Force Headquarters (DJFHQ) (L), Enoggera QLD | Doc Data Sheet |
| **Joint Operations Command** | |
| Director General Joint Operations | Doc Data Sheet |
| Chief of Staff Headquarters Joint Operations Command | Doc Data Sheet |
| Commandant ADF Warfare Centre | Doc Data Sheet |
| Director General Strategic Logistics | Doc Data Sheet |
| COS Australian Defence College | Doc Data Sheet |
| **Intelligence and Security Group** | |
| AS Concepts, Capability and Resources | 1 |
| DGSTA , Defence Intelligence Organisation | 1 Printed |

| | |
|---|---|
| Manager, Information Centre, Defence Intelligence Organisation | 1 |
| Director Advanced Capabilities | Doc Data Sheet |

**Defence Materiel Organisation**

| | |
|---|---|
| Deputy CEO | Doc Data Sheet |
| Head Aerospace Systems Division | Doc Data Sheet |
| Head Maritime Systems Division | Doc Data Sheet |
| Program Manager Air Warfare Destroyer | Doc Data Sheet |
| CDR Joint Logistics Command | |
| Guided Weapon & Explosive Ordnance Branch (GWEO) | Doc Data Sheet |

**OTHER ORGANISATIONS**

| | |
|---|---|
| National Library of Australia | 1 |
| NASA (Canberra) | 1 |
| Library of New South Wales | 1 |

**UNIVERSITIES AND COLLEGES**

**Australian Defence Force Academy**

| | |
|---|---|
| Library | 1 |
| Head of Aerospace and Mechanical Engineering | 1 |
| Hargrave Library, Monash University | Doc Data Sheet |

**OUTSIDE AUSTRALIA**

**INTERNATIONAL DEFENCE INFORMATION CENTRES**

| | |
|---|---|
| US Defense Technical Information Center | 1 |
| UK Dstl Knowledge Services | 1 |
| Canada Defence Research Directorate R&D Knowledge & Information Management (DRDKIM) | 1 |
| NZ Defence Information Centre | 1 |

**ABSTRACTING AND INFORMATION ORGANISATIONS**

| | |
|---|---|
| Library, Chemical Abstracts Reference Service | 1 |
| Engineering Societies Library, US | 1 |
| Materials Information, Cambridge Scientific Abstracts, US | 1 |
| Documents Librarian, The Center for Research Libraries, US | 1 |

| | |
|---|---|
| SPARES | 5 Printed |

**Total number of copies: 37 Printed: 16 PDF: 21**

**DEFENCE SCIENCE AND TECHNOLOGY ORGANISATION**
**DOCUMENT CONTROL DATA**

1. PRIVACY MARKING/CAVEAT (OF DOCUMENT)

2. TITLE

Development and Calibration of a Frangible Leg Instrumented for Compression and Bending

3. SECURITY CLASSIFICATION (FOR UNCLASSIFIED REPORTS THAT ARE LIMITED RELEASE USE (L) NEXT TO DOCUMENT CLASSIFICATION)

| | |
|---|---|
| Document | (U) |
| Title | (U) |
| Abstract | (U) |

4. AUTHOR(S)

M.J. Footner, D.M. Bergeron and R.J. Swinton

5. CORPORATE AUTHOR

DSTO Defence Science and Technology Organisation
PO Box 1500
Edinburgh South Australia 5111 Australia

| 6a. DSTO NUMBER | 6b. AR NUMBER | 6c. TYPE OF REPORT | 7. DOCUMENT DATE |
|---|---|---|---|
| DSTO-TR-1829 | AR-013-583 | Technical Report | February 2006 |

| 8. FILE NUMBER | 9. TASK NUMBER | 10. TASK SPONSOR | 11. NO. OF PAGES | 12. NO. OF REFERENCES |
|---|---|---|---|---|
| 2004/1031440/1 | ARM 04/025 | DGLD | 54 | 6 |

13. URL on the World Wide Web

http://www.dsto.defence.gov.au/corporate/reports/DSTO-TR-1829.pdf

14. RELEASE AUTHORITY

Chief, Weapons Systems Division

15. SECONDARY RELEASE STATEMENT OF THIS DOCUMENT

*Approved for public release*

OVERSEAS ENQUIRIES OUTSIDE STATED LIMITATIONS SHOULD BE REFERRED THROUGH DOCUMENT EXCHANGE, PO BOX 1500, EDINBURGH, SA 5111

16. DELIBERATE ANNOUNCEMENT

No Limitations

17. CITATION IN OTHER DOCUMENTS Yes

18. DSTO RESEARCH LIBRARY THESAURUS

Landmines; Frangible Surrogate Leg (FSL); Non-destructive drop test; Calibrations; PE4 charges, Explosive input

19. ABSTRACT

In order to quantify the loads transferred to a human leg during a landmine explosion, the lower portion of the Frangible Surrogate Leg (FSL) was modified to incorporate a load sensor. This report describes these modifications and the work carried out to calibrate the response of the modified FSL (FSLM) to static and dynamic loads. Non-destructive drop tests were performed to characterise repeatability from test to test for a given specimen, as well as the variation of response between specimens. Upon completion of these calibrations, five FSLM specimens were subjected to the explosion of 50-gram PE4 charges buried in sand. The standoff between the specimens and the soil surface ranged from 50 mm to 200 mm. The results demontrated how variations of the explosive input affects the load transmitted to the specimens and the resulting level of damage.